Published in final edited form as:
Inorg Chem. 2008 February 4; 47(3): 1053–1066. doi:10.1021/ic701920v.

Oxygen-Centered Hexatantalum Tetradecaimido Cluster Complexes

Jamin L. Krinsky, **Laura L. Anderson**[†], **John Arnold**[*], and **Robert G. Bergman**[*]
Department of Chemistry, University of California, Berkeley, California 94720

Abstract

The syntheses and characterization of several octahedral hexatantalum cluster compounds of formula $(ArN)_{14}Ta_6O$ are described (Ar = Ph, *p*-MeC_6H_4, *p*-$MeOC_6H_4$, *p*-*t*-BuC_6H_4, *p*-BrC_6H_4, *m*-ClC_6H_4). Treatment of $Bn_3Ta{=}N$-*t*-Bu (Bn = $CH_2C_6H_5$) or pentakis(dimethylamido)tantalum with an excess of the appropriate aniline and stoichiometric water or tantalum oxide afforded varying yields of arylimido clusters. The structures of two species were confirmed by X-ray diffraction (XRD), while the identity of the central oxygen atom was elucidated by electrospray mass spectrometry (MS) using $^{17}O/^{18}O$-enriched material. The title species are very air- and moisture-sensitive but quite thermally stable in solution. Experimentally determined optical properties and oxidation/reduction potentials, as well as some computational results, indicate that they possess an electronic structure wherein the highest occupied molecular orbitals are ligand-centered, while the lowest unoccupied orbitals are metal-centered and delocalized throughout the tantalum cage. Whereas chemical oxidation resulted in cluster decomposition, reduction with decamethylcobaltocene yielded stable salts of formula $[Cp^*_2Co][(ArN)_{14}Ta_6O]$ (Ar = Ph, Ar = *p*-MeC_6H_4). Small-molecule reactivity studies on one of these clusters showed that its imido functionalities are moderately reactive toward oxide donors but inert with respect to metallaheterocycle-forming processes. Clean imido/oxo exchange was observed with aldehydes and ketones, leading cleanly to organic imines with no soluble byproducts being observed. This exchange was also observed with a rhenium oxo compound (generating an imidorhenium complex as the only soluble species). All 14 imido groups were transferred in these reactions, and no mixed-ligand cluster intermediates were ever observed.

Introduction

A thorough understanding of multiple bonding between transition metals and nitrogen ligands is of great theoretical and commercial interest. Imido complexes are known for the majority of the d-block metals, and a wide range of substitution on the imido ligands has been demonstrated.1 The properties of the metal–nitrogen bond vary greatly with differences in the steric and electronic environment: while the imido functionalities in Schrock's molybdenum olefin metathesis catalysts are chemically inert and serve as supporting ligands,2 terminal imido bonds to many early and late transition metals are extremely reactive.3 Imido complexes have been postulated as intermediates in several catalytic processes including aziridination4 and hydroamination,5 and in the latter case, isolated group 4 metal–imido compounds have been shown to be catalytically active.6

[*] To whom correspondence should be addressed. E-mail: arnold@berkeley.edu (J.A.), rbergman@berkeley.edu (R.G.B.).
[†]Current address: Department of Chemistry, University of California, Irvine, CA 92697.

Supporting Information Available: CIF-format files for all crystallographically determined structures, experimental procedures for alternate syntheses of **2**, **3**, and **7** as well as syntheses of **12**–**14**, additional ESI mass spectra of **3**, **3**($^{17,18}O$), **4**, and **4**($^{17,18}O$), and positional coordinates of all computed structures. This material is available free of charge via the Internet at http:/pubs.acs.org.

Work in our research groups has extended hydroamination chemistry to group 5 metals, using neutral and cationic alkyltantalum imides as catalysts.7,8 During these studies it was discovered that the reaction of the hydroamination catalyst $Bn_3Ta{=}N\text{-}t\text{-}Bu$ (**1**) with aniline yielded a bright red, polynuclear tantalum species of uncertain composition (compound **2**, eq 1). A partial structural determination by X-ray diffraction9 showed that **2** appeared to consist of an octahedron of six tantalum atoms, surrounded by six terminal and eight facially bridging phenylimido ligands (Figure 1). A central atom was located but its identity could not be assigned on the basis of the available data, and a large amount of residual election density was observed in the unit cell suggesting the presence of additional species.10

$$\underset{\mathbf{1}}{Bn_3Ta{=}N\text{-}t\text{-}Bu} + \underset{5\ \text{equiv}}{PhNH_2} \xrightarrow[24\ h]{135\ ^\circ C,\ C_6H_6} \underset{\mathbf{2}}{\text{red crystals}} \quad (1)$$

Many hexanuclear transition metal clusters are present in the literature; however, such dense packing of organic ligands on these species is quite uncommon.11 The closest analogues are the polyimido hexamolybdates and hexatungstates prepared by treatment of the corresponding oxo clusters with isocyanates.12 In these cases only the terminal oxo moieties were replaced by imido or hydrazido groups, and thus to our knowledge no other hexanuclear clusters have been reported which contain alkyl- or arylimido ligands at all terminal and bridging sites.13

That such a novel cluster complex appears to be a thermodynamic sink under the conditions in which it forms was intriguing to us, and thus we wished to gain an understanding of its properties as well as its exact identity. The characterization of **2** and a few substituted derivatives, as well as preliminary results pertaining to their physical and chemical properties, was recently communicated.14 Herein we report a more complete account of the synthesis and characterization of a family of cluster compounds of general formula $(ArN)_{14}Ta_6O$. Experimentally and computationally derived insights into their geometric and electronic configurations are presented in detail, in addition to new results concerning their chemical reactivity.

Results and Discussion

Synthesis and Characterization of $(PhN)_{14}Ta_6O$ (2)

As stated above, the reaction of $Bn_3Ta{=}N\text{-}t\text{-}Bu$ (**1**) with excess aniline yielded a bright red, sparingly soluble crystalline material possessing the initially tentative formula $(PhN)_{14}Ta_6O$ (**2**). If this assignment were correct, a source of oxygen would be necessary for the formation of **2**. Given the low and irreproducible yields obtained in its synthesis, the identity of this adventitious oxygen source was at first uncertain. Organic oxygen sources such as peroxides, pyridine *N*-oxide, or phosphine oxides failed to yield **2**. Likewise, negligible quantities of **2** were isolated when very pure starting materials were used and the glassware was freshly washed with HF (Table 1, entry 1). While addition of a substoichiometric quantity of oxygen after heating the reaction mixture afforded **2** when the reaction was run on very small scale, this method was not effective on a preparative scale (Table 1, entry 3). However, when partially oxidized (old) samples of **1** were employed, a consistent yield was obtained (Table 1, entry 4). It was finally discovered that the addition of water (0.2 equiv relative to tantalum) to the reaction mixture before heating at 135 °C greatly increased the product yield (Table 1, entry 6). Because the alkyltantalum starting material **1** is extremely

moisture sensitive, the added water must generate tantalum oxo species that subsequently donate an oxide to a reactive intermediate during the cluster-formation process. Indeed, a small amount of white precipitate was always observed in the reaction mixture after the addition of water.

Occasionally, a large amount of crystalline **2** was deposited above the solution on the walls of the reaction vessel during heating. When the vessel was agitated so that the crystals redissolved, that quantity of product was not isolated upon cooling the reaction mixture. Subsequent studies indicated that in general the reaction side products greatly increase the solubility of the desired product, making crystallization from the reaction mixture very inefficient. Following this lead, the highest yields of **2** (up to 57%, Table 1, entry 8) were obtained by decreasing the solvent polarity such that the product precipitated as it was formed at high temperature. Compound **2** is much less soluble than the other products, and thus, the only necessary purification step was the facile mechanical separation of the white precipitate (formed after water addition) from the microcrystalline product. Tantalum oxide was also moderately effective as an oxygen source (Table 1, entry 9). Because air and water were rigorously excluded from the reaction conditions employed previously, varying quantities of residual tantalum oxide remaining on the walls of the reaction vessels must have been responsible for the variable cluster yield obtained in those cases. It had been assumed that Ta_2O_5 was no more reactive than the Pyrex vessels themselves and thus was sometimes allowed to accumulate from one run to the next. There is evidence that even silica can act as an oxide donor, as a few crystals of cluster were sometimes observed in reaction mixtures contained in flame-sealed NMR tubes, wherein all other sources of oxygen were carefully excluded.

Establishing conditions for the growth of high-quality crystals of **2** was nontrivial; the only crystals of sufficient size that could be grown during the initial stages of this investigation were of moderate quality, resulting in a problematic X-ray diffraction data set. More recently, a single-crystal synchrotron15 X-ray diffraction apparatus became available to us, enabling the analysis of very small crystals of **2** grown from benzene. A high-quality data set was obtained, and structural solution yielded the centrosymmetric octahedral structure observed previously (Figure 2). The crystal lattice has the space-group symmetry $P\bar{1}$, with the central atom occupying the inversion center. Compound **2** possesses the Ta_6O core of hexatantalate ($Ta_6O_{19}^{8-}$)16 but with all of the terminal and edge-bridging oxo ligands replaced by terminal and facially bridging phenylimido ligands.

In the solid state, the Ta_6O cluster core is slightly distorted from O_h symmetry and the phenylimido ligands pack so that the potential D_{2d} symmetry is not realized. The Ta–O distances are shorter than those in hexatantalate, measuring 2.2079(4), 2.2035(5), and 2.2119(4) Å for Ta1, Ta2, and Ta3, respectively. This significant, though small, anisotropy in the cluster core is recurrent in these compounds. It is unclear if this is the result of a second-order Jahn–Teller effect or simply a geometric consequence of maximizing bonding between the tantalum centers and the bridging imido ligands. The published structure of hexatantalate mentioned above is unfortunately not of sufficient quality to determine whether this subtle effect is also present in that system. In contrast to the Ta–O distances, the $Ta–N_{terminal}$ distances of 1.790(3) (Ta1–N3), 1.793(4) (Ta2–N4), and 1.791(4) Å (Ta3–N7) are all equivalent within error. One of the three unique $Ta–N_{terminal}–C_{phenyl}$ bond angles deviates significantly from 180°, with a C31–N3-Ta1 angle of 172.1(4)°. This appears to be the result of a close intermolecular contact and is not indicative of any internal electronic effect.

The only additional species observed in the unit cell are four molecules of benzene. If the assignment of the central atom as oxygen were incorrect, the cluster should carry a charge

and thus a counterion would be present. These data, taken together with the synthetic results, strongly indicated that the central atom in **2** is indeed oxygen. However, a stereochemically inactive proton (providing charge balance for an anionic cluster) would not be observed by the methods discussed above and so some form of direct detection was needed for an unambiguous assignment.

Mass spectrometry was an attractive technique because it can very accurately determine the mass of a substance, thus distinguishing between compounds of very similar composition. While the observation of a molecular ion of the correct mass would be quite convincing, a change in mass with different isotopically labeled oxide centers would be superior. To this end, samples of substituted analogs (p-tolN)$_{14}$Ta$_6$O (**3**) (p-tol = p-MeC$_6$H$_4$) and (p-MeOC$_6$H$_4$N)$_{14}$Ta$_6$O (**4**) (syntheses are discussed below) were prepared by following the procedure discussed above but using water enriched in ^{17}O and ^{18}O. Of the mass spectrometry methods available, all presented difficulties when evaluated for their utility with respect to this system. Simple electron impact MS is generally not suitable for compounds of such size, and soft ionization techniques usually require the use of a matrix containing functionality not compatible with reactive early metal complexes. With this in mind, electrospray ionization (ESI) mass spectrometry was attempted using only THF as a matrix.

Due to extensive cluster fragmentation and subsequent reaction with the THF matrix, no molecular ions were observed. Indeed, none of the observed fragments corresponded to combinations of the cluster core and arylimido fragments. However, many of the high molecular weight fragments (up to ca. 2000 Da) possessed masses 16 Da greater for **4** (MeO) than for **3** (Me) (Figure 3, additional spectra available in the Supporting Information). Therefore, these fragments apparently each retained one imido ligand. Although informative, analysis of these nonlabeled samples did not provide any evidence of the nature of the central cluster atom. Samples of **3** and **4** enriched in ^{17}O and ^{18}O (**3**(^{17,18}O), **4**(^{17,18}O)), however, provided a convincing result. As shown in Figure 3, each high-mass fragment from the nonlabeled cluster was accompanied by fragments that were 1 and 2 Da heavier, including those that were inferred to still possess an imido ligand.

These extra peaks can only be attributed to the presence of heavier isotopes of oxygen, as the labeled and nonlabeled samples were prepared in exactly the same manner with the same batches of starting materials (excepting water). Both labeled and nonlabeled samples were of high purity and crystalline, ruling out the presence of significant amounts of tantalum oxide that could also be isotopically enriched in labeled samples. While this unconventional methodology provided correspondingly unconventional results, the data provide convincing evidence for assignment of these compounds as oxide-centered clusters.

Reaction Scope in Tantalum Source and Amine

Given that the only fragment of **1** retained in the product cluster is the tantalum ion, any tantalum complex capable of exchanging all of its ligands with arylimido (and oxo) ligands should be an effective synthon. Moreover, a more synthetically accessible starting material would be very desirable, especially considering that the percent yields of product diminished when the reaction was scaled above 100 mg of **1**. A preliminary screen of alternate metal sources showed that halide-containing complexes such as (pyridine)$_2$Cl$_3$Ta=N-t-Bu or TaCl$_5$ did not afford the desired product. This is probably due to the inability of aniline to fully replace the tantalum-bound chlorides. As anticipated, it was confirmed that tantalum oxide itself is ineffective as a tantalum source, only functioning as an oxide source under the reaction conditions.

Turning to species with more reactive ligands, it was found that commercially available pentakis(dimethylamido)tantalum ($Ta(NMe_2)_5$) provided acceptable yields of **2**. Additionally, this reagent enabled the development of a large-scale synthesis of **2**, producing useful quantities of product after several days at reflux in toluene (eq 2). While the percent yields were lower than the best obtained at small scale using **1**, they did not drop off with increasing reaction scale.

$$\underset{1\text{ g}}{Ta(NMe_2)_5} + \underset{6\text{ equiv}}{\text{aniline}} + \underset{1/6\text{ equiv}}{H_2O} \xrightarrow[\text{toluene}]{\text{reflux, 4 d}} \underset{38\%}{\mathbf{2}} \quad (2)$$

Screening of a set of commonly encountered amines revealed that certain substituted anilines also afforded the corresponding imido clusters (Scheme 1). The arylamines *p*-toluidine and *p*-anisidine provided $(p\text{-tolN})_{14}Ta_6O$ (**3**) and $(p\text{-MeOC}_6H_4N)_{14}Ta_6O$ (**4**) (introduced earlier) isolated in 48% and 49% yield, respectively, using **1** as starting material. Compound **3** was also prepared on a larger scale (625 mg, 20%) using $Ta(NMe_2)_5$ as described above and proved to be the most synthetically useful of the derivatives presented here. In this case it was necessary to employ a mixture of toluene and *n*-octane as solvent to force the product to precipitate from the reaction mixture upon cooling. Under these conditions tantalum oxide proved to be preferable to water as an oxide source. The extremely soluble $(p\text{-}t\text{-BuC}_6H_4N)_{14}Ta_6O$ (**5**) was also successfully prepared but in very poor isolated yield (2%). Product isolation required that the reaction be performed in pure *n*-octane, which resulted in a precipitate of complex composition. After the sample was washed with pentane, this precipitate was extracted with Et_2O, affording a small amount of material that required much further washing with pentane before it could be successfully crystallized.

Halide-substituted anilines proved problematic, as their corresponding imido clusters were either highly insoluble or exhibited solubilities similar to those of the unwanted byproducts. Of the ones investigated, only *p*-bromoaniline and *m*-chloroaniline provided an isolable product, $(p\text{-BrC}_6H_4N)_{14}Ta_6O$ (**6**) and $(m\text{-ClC}_6H_4N)_{14}Ta_6O$ (**7**) in 4% and 15% yield, respectively. In both cases the principal factor responsible for the low yield was the difficulty with which the product was separated from the reaction mixture.

While the insolubility of isolated **7** precluded spectroscopic characterization, high-quality crystals were obtained from a reaction mixture and subjected to X-ray diffraction analysis (Figure 4). The structure is analogous to that of **2** but with two molecules of $t\text{-BuNH}_2$ and two molecules of benzene present in the unit cell. The packing of the aryl substituents is remarkably ordered, with only one of the seven unique *m*-chlorophenyl groups disordered between two positions related by an approximate 2-fold rotation about the aryl C–N bond. The Ta–O distances in **7** are 2.1741(2), 2.1808(2), and 2.1658(2) Å for Ta1, Ta2, and Ta3, respectively. These bond distances are slightly contracted (Δ_{ave} = 0.034 Å) relative to those of **2**, while the $Ta–N_{terminal}$ bond distances are slightly longer than those of **2**, measuring 1.811(4) (Ta1–N1), 1.806(4) (Ta2–N2), and 1.811(4) Å (Ta3–N3).

Cluster compounds arising from $p\text{-Me}_2NC_6H_4NH_2$ and 4-aminobiphenyl were apparently observed in solution but proved inseparable from the reaction byproducts. On one occasion, a small quantity of $(p\text{-Me}_2NC_6H_4N)_{14}Ta_6O$ (**8**) was isolated in reasonably pure form, but the purification method proved irreproducible and only ^1H NMR data supported its formulation. Other halogenated anilines afforded intractable mixtures that did not appear, by

NMR, to contain the desired products. In contrast to *p*-bromoaniline, attempted cluster synthesis using *p*-iodoaniline resulted only in black tars. It seems that cluster formation from electron-poor anilines is generally disfavored, as 3,5-fluoroaniline, *p*-trifluoromethylaniline, *p*-nitroaniline, 4-aminostyrene, 4-aminobenzonitrile, and 4-aminopyridine were all ineffective amine sources under the conditions investigated. Finally, only arylamines were tolerated: neither benzylamine nor isopropylamine afforded the desired alkylimido clusters.

When **1** was treated with excesses of both *p*-toluidine and *p*-anisidine simultaneously, a material was obtained that appeared by ^{1}H NMR and APCIMS17 to consist of a mixture of compounds possessing the formula $(p\text{-MeOC}_6\text{H}_4\text{N})_n(p\text{-tolN})_{14-n}\text{Ta}_6\text{O}$. The ratios of *p*-anisyl to *p*-tolyl groups corresponded to a Gaussian distribution centered at about $n = 9$. Thus, the two anilines react at competitive rates, but it appears that electron-rich anilines are preferred although more competition experiments would be needed to confirm this. By ^{1}H NMR there appears to be no preference for *p*-anisyl or *p*-tolyl substitution in the terminal or bridging positions, as the overall ratios of terminal to bridging resonances were still 6:8 for both the MeO and Me signals. Separation of the species by crystallization was not possible: beautifully faceted, dark purple crystals were always obtained which contained the same distribution of cluster substitution present in the supernatant.

Physical Properties, Experimentally Determined

Compounds **2**–**7** are thermally stable, extremely air- and moisture-sensitive crystalline solids. In solution, the more electron-rich **3**–**5** decomposed over several days if stored in polypropylene-capped vials inside an inert-atmosphere glove-box. Nonetheless, a sample of **3** in C_6D_6 showed no decomposition after it was heated at 200 °C for 2 weeks in a flame-sealed NMR tube. Thus, in the absence of a reaction partner these compounds appear to exist in their thermodynamically favored configuration. The symmetrical structure allows each electropositive tantalum center to access the lone available oxo ligand, and the arylimido ligands are arranged to maximize bonding with the Ta_6O core.

Compound **2** is sparingly soluble in aromatic solvents and only moderately so in THF, which is not surprising considering the presence of a closely packed array of unsubstituted phenyl rings. While **3** and **4** are considerably more soluble, the 14 methyl groups only increase their solubility to about 10 mM in benzene and slightly more in THF. Substitution of the methyl groups for *tert*-butyl groups in **5**, however, increases the compound's solubility to the extent that it is very soluble in Et_2O and slightly soluble in pentane. Halogenated compounds **6** and **7** differ greatly in their solubility, with **6** exhibiting good solubility in THF, but not in aromatic solvents, and **7** resisting dissolution in all nonreactive organic solvents once isolated in pure form.

As stated above, the most-symmetric conformation of **2** would have D_{2d} symmetry. While only inversion symmetry was observed in the solid-state structure, NMR spectra showed apparent O_h symmetry with two sets of aryl signals corresponding to the terminal and facially bridging sites (Figure 5). Thus, the imido aryl groups must rotate rapidly relative to one another so that the effective electronic environment on each side of each aryl group is equivalent. From inspection of the solid-state structure, it is apparent that the aryl groups are sufficiently close to one another that they should not be free to rotate completely independently, and so there should be some barrier to aryl group rotation. This barrier must be very low, however, as ^{1}H NMR spectra showed no broadening or decoalescence of signals when a sample of **5** in THF-d_8 was cooled to −100 °C.

Compound hues vary from red/orange (**7**) to cherry red for the alkyl-substituted **3** and **5**, to red/black for the more electron-rich **4**. The very electron-rich **8** possesses a deep brown/black color. Bromide substitution in the *para* position of a phenyl ring presents an

ambiguous situation electronically, but the deep crimson hue of **6** suggests that in this case the bromide substituents are moderately electron-donating. Compounds **2**–**4** exhibit intense UV absorptions only slightly red-shifted from those of the anilines from which they are derived (Figure 6). However, in contrast to aniline these compounds also show charge-transfer bands in the visible region, with onsets of about 600 nm (Figure 6 insert). Both features are more red-shifted with increasingly electron-rich substitution. Also unlike aniline, fluorescence measurements detected no emission between 300 and 1000 nm using a range of excitation wavelengths. The large number and density of vibrational modes accessible to these clusters probably makes internal conversion and subsequent thermal relaxation the dominant excited-state decay pathway.

Because the clusters are formally d_0 tantalum compounds, the charge-transfer excitations discussed above should be ligand-to-metal charge transfers. The UV–vis data for **2**–**4** indicate that this transition is facile and thus the cluster LUMO should be relatively low-lying. This could be the case if the LUMO were a combination of d orbitals located on more than one tantalum center, providing a delocalized and thus stabilized molecular orbital.

Data obtained from analysis of **3** by cyclic voltammetry are consistent with this bonding scenario (Figure 7). A reversible reduction was observed at −1.44 V (vs Fc/Fc^+ couple, Fc = ferrocene), indicating that relatively mild reducing agents should chemically reduce **3** in THF. An additional reduction occurred at −2.14 V; however, its reversibility is uncertain due to its position so near the potential limit of the solvent. There were also two irreversible oxidations, one at 0.01 V and one at 0.27 V. Therefore, **3** displays a first oxidation potential nearly identical with that of ferrocene; however, the cations produced are apparently very unstable.

Physical Properties, Computed by Hybrid DFT

The physical properties discussed in the previous section suggest a cluster bonding scheme wherein the high-lying populated orbitals are ligand-centered, in analogy with mononuclear d_0 metal complexes. However, the ease with which **3** is reduced and the intense visible-region absorption bands indicate that the LUMOs of the clusters are stabilized relative to their monomeric relatives. With the hope of a better understanding concerning the nature of this stabilization, electronic structure calculations at the X3LYP18/LACVP* level of theory were performed using the crystallographically determined coordinates of **2**. Figure 8 depicts the HOMO of **2**, one of three nearly degenerate molecular orbitals that would possess t_g symmetry were the cluster perfectly octahedrally symmetric. As expected, these orbitals are purely imido ligand-centered, consisting of linear combinations of fragment orbitals analogous to the HOMO of aniline. The majority of the electron density resides on the bridging imido nitrogens, and each imido fragment orbital is weakly antibonding with its closest neighbors.

In analogy to mononuclear d_0 metal complexes, the lowest unoccupied MOs of **2** are metal-centered (Figure 9), with no contributions from the imido fragments or central oxide. However, in this case the LUMOs are linear combinations of d orbitals from all six tantalum centers and, thus, if populated, the electron density would be much more delocalized than in mononuclear complexes. These two LUMOs are nearly degenerate and would form a set of e_g symmetry if the cluster were truly octahedral. Therefore, the orbital scheme is analogous to that of a d_6 octahedral species wherein the frontier orbitals consist of a filled, triply degenerate set and a doubly degenerate virtual set. The difference is that here the t set is ligand-centered and the octahedral symmetry corresponds to the cluster as a whole instead of a single metal center.

Closer inspection of the LUMOs of **2** reveals that the LUMO possesses a slightly bonding combination of d orbitals about two meridians defined by four tantalum centers each, while the combination is slightly antibonding about the third meridian. The LUMO+1 possesses a bonding combination about one meridian only. Thus, population of the former orbital might result in a Jahn–Teller distortion wherein two opposite Ta–O distances are contracted, while population of the latter would have the opposite effect.

The above discussion provides some explanation for the observed properties of **2**. We wished to extend this investigation to compounds for which no experimentally determined structure was available, and so geometry optimizations were performed on models of **3**, **4**, and a hypothetical complex bearing electron-withdrawing 4-pyridylimido ligands, $(NC_5H_4N)_{14}Ta_6O$ (**9**). As a control experiment, **2** was first optimized both under the constraint of inversion symmetry and with no geometric constraints. While the $Ta–N_{terminal}$ bond distances in optimized **2** are essentially identical with the experimentally determined values, the calculated Ta–O distances average 0.016 Å longer. This discrepancy is possibly due to the lack of polarization functions in the basis set used for tantalum, but larger basis sets proved prohibitively expensive in this large system. Both optimized structures exhibited MO surfaces and energies very similar to those calculated from the experimentally determined structure, and thus, the substituted models were subsequently optimized using inversion symmetry as a constraint (greatly reducing computational cost). Positional coordinates of the optimized structures are available in the Supporting Information.

Given the potential shortcomings of DFT in reproducing meaningful energy values, the energies listed in Table 2 should not be directly compared with any observed values of physical properties.19 However, because the four species compared here are so similar, clear trends in energy level changes with changing ligand substitution should be reasonably reliable. In the order from electron-poor **9** to electron-rich **4**, the HOMO energy increases by 2.25 eV while the LUMO energy increases by only 1.77 eV. This results in a decrease of the HOMO–LUMO energy gap with increasing electron-donating ability of the arylimido substituents. In a qualitative sense the antibonding, ligand-centered HOMO is more destabilized than the metal-centered LUMO by the presence of increasingly electron-rich ligands. These data provide a theoretical rationale for the experimentally observed red-shifts in the UV–visible absorption bands.

Chemical Reactivity Studies

Observations and calculations relating to electronic structure suggested that the title compounds should be reactive toward chemical oxidants and reductants, and treatment with the latter might yield stable anionic cluster compounds. When compounds **2** and **3** were treated with silver trifluoromethanesulfonate (OTf), dark tars were obtained which displayed no observable signals in their ^{1}H NMR spectra (Scheme 2). This result is consistent with cluster oxidation by silver(I), which was predicted to yield reactive organic-centered radical cations. Chemical reduction of **2** and **3** by decamethylcobaltocene (Cp^*_2Co), however, provided isolable decamethylcobaltocenium salts of formula $[Cp^*_2Co][(ArN)_{14}Ta_6O]$ (Ar = Ph (**10**), Ar = *p*-tol (**11**)) in good yield.

Compounds **10** and **11** are green/brown solids that form brown solutions, although they are sparingly soluble in THF and insoluble in aromatic solvents. Signals in their ^{1}H NMR spectra are broad but within the normal diamagnetic chemical shift range. The absence of a signal at ca. 45 ppm corresponding to neutral Cp^*_2Co confirmed that it had been oxidized to its diamagnetic cation (the signal for which was present at ca. 2 ppm). Magnetic moment measurements on a solid sample of **11** yielded a μ_{eff} value of 1.78 μ_B, which is very close to

the theoretical spin-only value of 1.73 expected for a system containing one unpaired electron.

The solid-state structure of **10** is depicted in Figure 10. As with the structure of **2**, the central oxide is located on an inversion center and thus the asymmetric unit contains only half of the cluster anion. The cobalt of the $Cp^*_2Co^+$ cation is also situated on an inversion center. The Ta–O distances in **10** are very similar to those in neutral **2**, measuring 2.2018(4), 2.2099(4), and 2.2120(4) Å. To ensure accurate comparisons, larger crystals of **2** were successfully grown from THF solution and its structure was redetermined using Mo Kα radiation, as was used for data collection on **10**. The redetermined Ta–O distances for **2** are 2.1949(4), 2.2096(4), and 2.2101(4) Å (CIF available in Supporting Information).

In a comparison of these two data sets, it is evident that no significant change in Ta–O distance accompanied reduction. Therefore, either the metal-centered, singly occupied molecular orbital (SOMO) in **10** is not sufficiently bonding in character to have an observable effect or that orbital is in fact nonbonding. The $Cp^*_2Co^+$ cation's Co–C bond distances of 2.041(9), 2.043(9), 2.043(9), 2.054(9), and 2.054(8) Å are in good agreement with those of other structurally determined $Cp^*_2Co^+$ salts.20 If electron transfer had not occurred, much larger Co–C distances corresponding to the neutral Cp^*_2Co would have been observed. This claim is supported by the computed average $d_{Co–C}$ values of 2.091 and 2.168 Å for $Cp^*_2Co^+$ and Cp^*_2Co, respectively (X3LYP/LACVP* geometry optimizations, positional coordinates are available in the Supporting Information). These data, together with the observed changes in solubility and spectroscopic properties upon treatment of **2** and **3** with Cp^*_2Co, provide strong evidence for the assignment of **10** and **11** as ionic compounds.

Because each tantalum center in these cluster compounds is coordinatively saturated and embedded in what was assumed to be a very bulky ligand set, it was not expected that the cluster imido groups would exhibit reactivity often observed in other early metal systems. A vacant cis coordination site is usually necessary for metallacycle formation by insertion of an unsaturated organic molecule across the metal–imido bond.21 While metathesis reactions may be feasible if metallacycle formation is only involved in the transition state, the unfavorable steric situation should impede any such reactivity. Accordingly, unsaturated molecules including phenylacetylene, isothiocyanates, isocyanates, and carbon monoxide did not react with **3** upon extended heating. Although treatment of **3** with carbon dioxide did produce *p*-tolNCO22 (eq 3), only trace quantities were observed by ^{1}H NMR after the reaction mixture was heated at 135 °C for 2 weeks. The observed reactivity is opposite to that of the molybdate system reported by Maatta, in which imidomolybdenum clusters were generated by treatment of hexamolybdate with isocyanates, generating carbon dioxide as a byproduct.23

$$\mathbf{3} + \underset{\text{excess}}{CO_2} \xrightarrow[C_6D_6]{135\ ^\circ C} \text{“}Ta_xO_y\text{”} + p\text{-}MeC_6H_4NCO \tag{3}$$

In contrast to reactions with the π-ligands discussed above, treatment of **3** with sterically nondemanding alcohols such as ethanol and phenol resulted in evolution of *p*-toluidine and the formation of tantalum alkoxide products. This reactivity is not surprising given the high water sensitivity of the title compounds. Multiple alkoxide complexes were formed in reactions employing small alcohols, none of which were isolated. Treatment with the more

bulky triphenylsilanol, however, yielded only two siloxide-containing products, as detected by ^{1}H NMR spectroscopy. The major product was easily crystallized from the reaction mixture and identified as the homoleptic siloxide $Ta(OSiPh_3)_5$ (**12**) (Scheme 3). The minor product, presumably containing the central oxide from **3**, was not successfully isolated in pure form. Compound **12** was also prepared by treatment of $Ta(NMe_2)_5$ with 5 equiv of triphenylsilanol. The crystallographically determined structure of **12** is shown in Figure 11. The geometry about the tantalum center is nearly perfectly trigonal bipyramidal with a noncrystallographic 3-fold rotation axis defined by the axial ligands. The bond angle between the axial siloxy ligands is 178.1(4)°, and the sum of the equatorial O–Ta–O angles is 360.0(7)°. The Ta–O bond lengths are slightly longer than those of $(t\text{-}Bu_3SiO)_3Ta{=}PPh$24 and $(t\text{-}Bu_3SiO)_3Ta{=}C{=}C{=}Ta\text{-}(t\text{-}Bu_3SiO)_3$,25 possibly due to steric pressure in **12**. Only a few other homoleptic tantalum siloxides have been reported previously, all containing only alkylsiloxy ligands, and none were crystallographically characterized.26 To our knowledge, none of the previously reported homoleptic alkoxy– or mixed-alkoxy–tantalum species are monomeric.27

The reactivity discussed above indicated that ligand substitution reactions at the cluster tantalum centers are sterically feasible. Hence, the lack of reactivity with isocyanates must be of electronic origin, possibly a result of the necessity of forming relatively high-energy carbodiimides. Investigations employing simple organic carbonyls appeared to confirm this postulate (Scheme 4). When compound **3** was treated with 14 equiv of benzaldehyde, quantitative conversion to benzaldehyde *p*-tolylimine was observed after 2 d at ambient temperature. Benzophenone was also reactive, providing the corresponding ketimine in quantitative yield (by ^{1}H NMR) after heating at 135 °C overnight. The only other product from these reactions was insoluble tantalum oxide. The α-hydrogen-bearing acetophenone also provided product but in decreased yield (75% by ^{1}H NMR). While the desired *β*-diketimine was observed in the reaction mixture after treatment of **3** with acetylacetone, free *p*-toluidine was present shortly after ketone addition and so the transformation probably followed the classical condensation route. In this case it appears that the cluster ligands were protonated by the acidic diketone and the resulting tantalum species simply acted as a Lewis acid and water scavenger. It has been known for some time that certain early metal imides undergo imido/ oxo exchange with aldehydes and ketones.28 However, these species are generally coordinatively unsaturated and also reactive toward isocyanates and carbon monoxide.

In addition to their reactivity with organic carbonyl compounds, some imido complexes have been shown to undergo imido/oxo exchange.29 This reaction is thermodynamically favored when the oxo complex contains a metal that is more electronegative than that of the imido species.30 Nonetheless, we were very surprised to find that **3** reacted with 14 equiv of $Cp^*Cl_2Re{=}O$ at 75 °C, forming $Cp^*Cl_2Re{=}N\text{-}p\text{-}tol$ (**13**) as the only soluble product (eq 4). A black, insoluble precipitate was also obtained. As no starting materials or other soluble products were present, this material must contain Cp^*Cl_2Re and *p*-tolylimido fragments as well as tantalum oxide. Compound **13** has been fully characterized and its identity confirmed by X-ray diffraction analysis (Figure 12). The structure is unremarkable, being closely analogous to that of the known $Cp^*Cl_2Re{=}N\text{-}t\text{-}Bu$.31

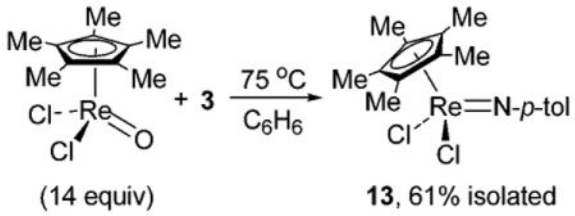

(4)

The oxo ligand of $Cp^*Cl_2Re{=}O$ resides close to the bulky Cp* ligand, and so there must be much more available space between the arylimido groups of **3** than was originally assumed. In fact, even the very sterically shielded **5** cleanly exchanged its imido ligands to afford $Cp^*Cl_2Re{=}N\text{-}p\text{-}C_6H_4\text{-}t\text{-}Bu$ (**14**). This reaction occurred very slowly at 75 °C but was complete after 12 h at 135 °C. There are two scenarios that would account for this reactivity: the arylimido groups could compact in a concerted manner so that a large hole is transiently formed in the ligand sphere; the clusters reversibly fragment in solution.

A number of experiments were performed to test for cluster lability. First, a solution of compound **3** was heated in the presence of excess *p*-anisidine, and separately a solution of **4** was heated in the presence of excess *p*-toluidine. Depending on the thermodynamic preference for electron-rich or electron-poor arylimido groups, one of these reaction mixtures should have produced a mixed-ligand species if the imido groups of **3** or **4** were thermally labile. No exchange was observed at temperatures at which the imido/oxo exchange reactions were performed (Scheme 5). There is evidence in the literature that acid can catalyze this type of reaction,32 but here the addition of anilinium triflate had no effect. An additional experiment involved heating an equimolar mixture of **3** and **4**. Again, no mixed-ligand clusters were observed.

A recurring observation provides some evidence for the ligand-compaction mechanism mentioned above: in all reactions resulting in oxide transfer to the cluster tantalum sites, no intermediate oxo/imido clusters were ever observed. Thus, the remaining 13 imido groups must have reacted very quickly after the first was exchanged. The only forthcoming explanation for this phenomenon is that the first substitution results in an area of little steric hindrance owing to the small size of an oxo ligand relative to an arylimide. With this hole opened in the ligand sphere, substrates could then access the tantalum–nitrogen linkages much more easily and thus each subsequent exchange would become progressively more facile.

Conclusions

A new type of polyatomic imido complex was fully characterized. The structure was confirmed by several X-ray diffraction experiments, and the identity of the cluster-core oxide was confirmed by mass spectrometry using isotopically labeled samples. Reproducible, acceptably high-yielding syntheses were developed for cluster species containing a variety of substituted arylimido ligands. Optical properties were found to vary with ligand substitution, resulting in red-shifts in the UV–visible spectra of more electron-rich species. Electronic structure calculations suggested that the phenomenon primarily arises from the destabilization of the ligand-centered HOMOs, while the tantalum-centered LUMOs are relatively unperturbed. Reactivity studies using one cluster derivative showed a surprising steric flexibility in the clusters' imido ligand sphere. Moderately bulky organic molecules were found to react with **3** at surprisingly low temperatures, provided the reaction

was strongly thermodynamically favored (e.g., exchange of imido ligands for oxo or alkoxy moieties).

Although this report provides a general overview of the title compounds, several issues have yet to be resolved. For example, evidence was presented indicating an energetic preference for electron-donating arylimido ligands, even while these substituents appear to be electronically destabilizing. Whether this preference is kinetic or thermodynamic is not currently known; indeed, the mechanism of cluster formation is entirely mysterious at present. The heterogeneity of the reaction mixture, as well as the polymeric nature of the initial arylamide substitution product, has so far precluded any thorough spectroscopic investigation. The fact that no well-defined intermediates were observed in NMR spectra during the course of the cluster-forming reaction suggests that the *closo*-hexatantalum architecture forms rapidly after the oxide moiety is trapped by some reversibly formed imido/ amido species. If conditions were developed under which the kinetics of the reaction could be determined, some information might be gained regarding the factors controlling cluster assembly. In addition, elucidation of the mechanism accounting for the quantitative exchange of imido and oxo groups between the cluster and a cyclopentadienyl(oxo)-rhenium complex may explain the absence of observable partially exchanged cluster intermediates in this reaction. Finally, the scope in metal source should be explored more fully. The discovery that this reaction is general for tantalum compounds containing only carbon and nitrogen ligands would have disturbing implications for the study of this element as a hydroamination or amidation catalyst, as these types of donors (cyclopentadienides, amides, etc.) are currently considered the most promising supporting ligands.

Experimental Section

General Methods

All manipulations were performed using standard Schlenk-line techniques or an N_2-atmosphere glovebox. Reactions followed by NMR spectroscopy were performed in 5 mm Pyrex NMR tubes which were flame-sealed under reduced pressure. Solvents were dried by passage through a column of activated alumina,33 degassed with nitrogen and stored over 4 Å molecular sieves. Solvents were tested with Na/benzophenone prior to use. Deuterated solvents were vacuum-transferred from Na/benzophenone or CaH_2 and stored in Teflon-sealed Kontes vessels inside a glovebox. NMR spectra were obtained with a Bruker DRX-500 spectrometer. Chemical shifts were calibrated relative to residual solvent peaks and are reported relative to TMS. UV–visible absorption spectra were recorded in THF on a Hewlett-Packard 8453 spectrophotometer using a 2 mm path-length cell. Elemental analyses were performed at the UC, Berkeley, CA, Microanalytical Facility with a Perkin-Elmer 2400 Series II CHNO/S analyzer. Electrospray mass spectrometry was performed by Dr. John Greaves at the UC, Irvine, CA, Mass Spectrometry Facility. Electrochemical investigations were performed on a BAS 100B electrochemical analyzer. Magnetic moment data were collected on a Quantum Design MPMS XL SQUID magnetometer. All starting materials obtained from commercial sources were used without further purification, except the anilines (distilled or sublimed prior to use). Compound **1**7 and $Cp^*Cl_2Re{=}O$34 were prepared as previously reported. Isotopically enriched water (30% ^{17}O, 50% ^{18}O) was purchased from Isotec and degassed prior to use.

Representative Procedure for X-ray Crystallography

A crystal of appropriate size was mounted on a Kaptan loop using Paratone-N hydrocarbon oil. The crystal was transferred to a diffractometer/CCD area detector,35 centered in the beam, and cooled by a nitrogen flow low-temperature apparatus that had been previously calibrated by a thermocouple placed at the same position as the crystal. An arbitrary

hemisphere of data was collected, and the raw data were integrated using SAINT.36 Cell dimensions reported were calculated from all reflections with $I > 10\sigma$. The data were corrected for Lorentz and polarization effects, but no correction for crystal decay was applied. Data were analyzed for agreement and possible absorption using XPREP.37 An empirical absorption correction based on comparison of redundant and equivalent reflections was applied using SADABS.38 The structure was solved via direct methods, expanded using Fourier techniques, and refined on F^2 with the SHELXTL-97 suite of programs.39 ORTEP diagrams were created using the ORTEP-3 software package40 and rendered in POV-ray.41 and 4.

Computational Methods

Molecular orbital calculations were performed using the Jaguar 6.5 package42 with Maestro 7.5 as the graphical user interface43 at the UC, Berkeley, CA, Molecular Graphics Facility. The hybrid DFT functional X3LYP44 was used throughout, which consists of the Becke three-parameter functional45 and the correlation functional of Lee, Yang, and Par.46 It also includes the Perdew–Wang 1991 gradient exchange functional,47 and the exchange has been parametrized to fit the Gaussian exchange density. We found that for this system the X3LYP functional gives results comparable to the well-known B3LYP48 but at slightly less computational cost. The LACVP* basis set was employed, which uses an effective core potential and valence double-ζ contraction basis functions for metals.49 The remaining atoms were treated with Pople's 6-31G* basis set, which includes a set of d polarization functions for non-hydrogen atoms.50 Single point energy calculations starting with the neutral cluster produced excited-state electronic configurations. Thus, the wave function was obtained by first calculating that of the dication using a level shift of 0.5 au. This wave function was then used as an initial guess for optimization of the neutral structure (level shift constraint removed). Unrestricted wave functions were used for the computations involving decamethylcobaltocene and its cation. Vibrational frequency calculations performed on the optimized structures (same level of theory) confirmed that they were true energetic minima. Graphical representations of MOs were generated in and exported from Maestro.

$(PhN)_{14}Ta_6O$ (2)

Pentakis(dimethylamido)tantalum (1.00 g, 2.49 mmol, 1 equiv) was dissolved in 5 mL of toluene. A solution of aniline (1.41 g, 15.14 mmol, 6.08 equiv) in 10 mL of toluene was added, followed by 7.5 μL (0.42 mmol, 0.16 equiv) of water. The mixture was heated at reflux for 4 d, after which time the flask was cooled to ambient temperature and the supernatant was removed. The solid was washed with Et_2O (2 × 10 mL) and then extracted with THF (2 × 20 mL). The extracts were combined and the solvent removed under vacuum, yielding 380 mg (0.158 mmol, 38%) of **2**. Crystals suitable for X-ray diffraction analysis were grown from concentrated solutions of benzene or THF. ^{1}H NMR (500 MHz, THF-d_8): δ 7.68 (dd, J = 8.5 Hz, 1.0 Hz, 16H, *o*-bridging *Ar*), 7.13 (m, 16H, *m*-bridging *Ar*), 6.98 (m, 12H, *m*-terminal *Ar*), 6.92 (m, 8H,*p*-bridging *Ar*), 6.71 (m, 6H, *p*-terminal *Ar*), 6.07 (dd, J = 8.5 Hz, 1.0 Hz, 12H, *o*-terminal *Ar*). ^{13}C{^{1}H} NMR (125.8 MHz, THF-d_8): δ 157.84, 156.83, 129.80, 129.20, 128.35, 126.87, 125.27, 124.86. UV/vis (THF): λ_{max}(onset) = 280 nm (580 nm). Anal. Calcd for $C_{84}H_{70}N_{14}OTa_6$: C, 42.09; H, 2.94; N, 8.18. Found: C, 42.23; H, 2.89; N, 8.86.

$(p\text{-}MeC_6H_4N)_{14}Ta_6O$ (3)

A Schlenk flask was charged with pentakis(dimethylamido)tantalum (3.00 g, 7.47 mmol, 1.00 equiv), Ta_2O_5 (200 mg, 0.452 mmol, 0.0605 equiv), and *p*-toluidine (2.41 g, 22.5 mmol, 3.01 equiv). Toluene (5 mL) was then added, followed by 15 mL of hexamethyldisiloxane. The mixture was heated at reflux for 4 d, after which time the flask

was cooled to ambient temperature and the supernatant was removed. The solid was washed with Et_2O (3 × 20 mL) and then extracted with 30 mL of hot THF. The THF solvent was removed under vacuum, yielding 625 mg (0.243 mmol, 20%) of **3** in good purity. ^{1}HNMR (500 MHz, C_6D_6): δ 8.03 (d, J = 8.5 Hz, 16H, *o*-bridging *Ar*), 6.87 (d, J = 8.0 Hz, 12H, *m*-terminal *Ar*), 6.81 (d, J = 8.5 Hz, 16H, *m*-bridging *Ar*), 6.47 (d, J = 8.0 Hz, 12H, *o*-terminal *Ar*), 2.08 (s, 18H, terminal Ar*Me*), 1.96 (s, 24H, bridging Ar*Me*). $^{13}C\{^1H\}$ NMR (125.8 MHz, C_6D_6): δ 155.49, 155.13, 134.25, 133.68, 130.18, 128.91, 126.78, 125.12, 21.17, 20.75. UV/vis (THF): λ_{max}(onset) = 285 nm (600 nm). Anal. Calcd for $C_{98}H_{98}N_{14}OTa_6$: C, 45.74; H, 3.84; N, 7.62. Found: C, 46.10; H, 4.08; N, 7.87.

(*p*-MeOC$_6$H$_4$N)$_{14}$Ta6O (4)

Compound **1** (100 mg, 0.190 mmol, 1 equiv) was dissolved in 1 mL of benzene. *p*-Anisidine (117 mg, 0.950 mmol, 5 equiv) was treated with 0.6 μL (0.03 mmol, 0.16 equiv) of degassed water via microsyringe, and the resulting mixture was dissolved in 0.5 mL of benzene. The two solutions were mixed, and the reaction mixture was transferred to a Kontes reaction vessel. Hexane (4 mL) was then added, causing the formation of a yellow precipitate. The vessel was sealed with a Teflon valve and immersed in a 135 °C oil bath. After a few minutes, most of the yellow solid had dissolved and the solution had developed a red color. After being heated for ca. 24 h, the reaction vessel was allowed to cool and was transferred to a glovebox. The supernatant was removed by pipet, and the crystalline product was washed with Et_2O (2 × 2 mL) and then pentane (2 × 2 mL). Isotopically enriched samples were prepared in an identical fashion using $^{17}O/^{18}O$-enriched water. Yield = 43.4 mg, 0.016 mmol, 49%. ^{1}H NMR (500 MHz, C_6D_6): δ 8.19 (d, J = 9.0 Hz, 16H), 6.74 (d, J = 9.0 Hz, 16H), 6.63 (s, 24H), 3.12 (s, 18H), 3.09 (s, 24H). $^{13}C\{^1H\}$ NMR (125.8 MHz, C_6D_6): δ 157.53, 157.45, 151.70, 151.63, 127.96, 126.22, 114.90, 113.75, 55.34, 55.17. UV/vis (THF): λ_{max}(onset) = 300 nm (630 nm). The product was recrystallized by pentane vapor diffusion into a benzene solution of **4** prior to submission for EA. Anal. Calcd for $C_{98}H_{98}N_{14}O_{15}Ta_6$: C, 42.07; H, 3.53; N, 7.01. Found: C, 42.62; H, 3.74; N, 6.90.

(*p*-*t*-BuC$_6$H$_4$N)$_{14}$Ta$_6$O (5)

A Schlenk flask was charged with pentakis(dimethylamido)tantalum (3.00 g, 7.47 mmol, 1.00 equiv) and Ta_2O_5 (200 mg, 0.452 mmol, 0.0605 equiv). *n*-Octane (20 mL) was then added, followed by *p*-*tert*-butylaniline (3.36 g, 22.5 mmol, 3.01 equiv). The mixture was heated at reflux for 4 d, during which time the yellow suspension became red in color. The supernatant was removed by filtration, and the orange solid was washed with cold pentane (40 mL). The residue was then extracted with Et_2O (3 × 10 mL). The extracts were combined and evaporated under reduced pressure, yielding a red solid. After being washed with 10 mL of pentane, the remaining solid was dissolved in 2 mL of Et_2O and placed in a vial which was nested in a larger vial containing pentane. After 2 d, the supernatant was removed by pipet and the pure **5** that had crystallized was washed with 5 mL of pentane (65 mg, 0.020 mmol, 1.6%). ^{1}H NMR (500 MHz, THF-d_8): δ 7.62 (d, J = 8.5 Hz, 16H), 7.18 (d, J = 8.5 Hz, 16H), 6.96 (d, J = 8.5 Hz, 12H), 5.98 (d, J = 8.5 Hz, 12H), 1.25 (s, 72H), 1.17 (s, 54H). $^{13}C\{^1H\}$ NMR (125.8 MHz, THF-d_8): δ 155.11, 154.93, 147.08, 146.82, 126.40, 126.19, 124.92, 124.56, 34.88, 34.68, 31.86, 31.84. Anal. Calcd for $C_{140}H_{182}N_{14}OTa_6$: C, 53.17; H, 5.80; N, 6.20. Found: C, 53.18; H, 5.98; N, 6.32.

(*p*-BrC$_6$H$_4$N)$_{14}$Ta$_6$O (6)

Pentakis(dimethylamido)tantalum (2.00 g, 4.98 mmol, 1.00 equiv) and *p*-bromoaniline (2.58 g, 15.0 mmol, 3.01 equiv) were mixed and dissolved in 10 mL of toluene. Water (15 μL, 0.84 mmol, 0.17 equiv) was then added by microsyringe, and the mixture was heated with stirring for 24 h. The reaction mixture was stirred while cooling to ambient temperature,

resulting in a fine orange precipitate. The solid was separated by filtration and washed with 100 mL of cold toluene. This residue was then extracted with hot toluene (5 × 10 mL), and each extract was cooled to −30 °C overnight, each yielding a small crop of crystalline **6** (127 mg combined, 0.0365 mmol, 4.4%). ^{1}H NMR (500 MHz, THF-d_8): δ 7.46 (d, J = 9.0 Hz, 16H), 7.42 (d, J = 9.0 Hz, 16H), 7.29 (d, J = 9.0 Hz, 12H), 6.02 (d, J = 9.0 Hz, 12H). ^{13}C{^{1}H} NMR (125.8 MHz, THF-d_8): δ 155.58, 155.09, 133.58, 132.12, 128.19, 126.48, 119.94, 119.24. Anal. Calcd for $C_{84}H_{56}Br_{14}N_{14}OTa_6$: C, 28.98; H, 1.62; N, 5.63. Found: C, 29.14; H, 1.51; N, 5.71.

(*m*-ClC$_6$H$_4$N)$_{14}$Ta$_6$O (7)

Compound **1** (100 mg, 0.190 mmol, 1 equiv) was dissolved in 1 mL of benzene. *m*-Chloroaniline (129 mg, 0.950 mmol, 5 equiv) was treated with 0.6 μL (0.03 mmol, 0.16 equiv) of degassed water via microsyringe, and the resulting mixture was dissolved in 0.5 mL benzene. The two solutions were mixed, and the reaction mixture was transferred to a Kontes reaction vessel. Hexane (4 mL) was then added, causing the formation of a yellow precipitate. The vessel was sealed with a Teflon valve and immersed in a 135 °C oil bath. After a few minutes, most of the yellow solid had dissolved and the solution had developed a red color. After being heated for ca. 24 h, the reaction vessel was allowed to cool and was transferred to a glovebox where the solvent was removed under vacuum. The orange oil was dissolved in 1 mL of toluene, into which pentane was allowed to diffuse. The resulting crystalline material was insoluble in compatible (nonreactive) solvents (13.4 mg, 0.0047 mmol, 15%). Anal. Calcd for $C_{84}H_{56}Cl_{14}N_{14}OTa_6$: C, 35.28; H, 1.97; N, 6.86. Found: C, 34.94; H, 2.17; N, 6.81.

[Cp*$_2$Co][(PhN)$_{14}$Ta$_6$O] (10)

Compound **2** (50 mg, 0.021 mmol, 1.0 equiv) was dissolved in 5 mL of boiling THF, and a 2 mL THF solution of decamethylcobaltocene (8.2 mg, 0.025 mmol, 1.1 equiv) was added. The reaction mixture immediately developed a deep, olive green color. Upon cooling to ambient temperature, the supernatant was decanted from the crystals of **10**·4THF that had formed (30 mg). Some of these crystals were of sufficient quality for use in X-ray diffraction analysis. The supernatant was heated to boiling, and 2 mL of pentane was slowly added. After standing at −30 °C for 2 d, an additional crop of crystals was recovered by decanting the supernatant and washing with Et_2O (46 mg total, 0.015 mmol, 73%). ^{1}H NMR (500 MHz, THF-d_8): δ 8.33 (br, 6H, *p*-terminal *Ar*), 8.13 (br, 12H, *o*-terminal *Ar*), 6.15 (br, 16H, *m*-bridging *Ar*), 5.74, 12H, *m*-terminal *Ar*), 4.80 (br, 8H, *p*-bridging *Ar*), 3.62 (v br, *o*-bridging *Ar*), 1.84 (v br, *Cp**). Peak assignments were determined by COSY NMR. Anal. Calcd for $C_{104}H_{100}CoN_{14}OTa_6 \cdot 4C_4H_8O$: C, 47.80; H, 4.41; N, 6.50. Found: C, 47.86; H, 4.36; N, 6.62.

[Cp*$_2$Co][(*p*-MeC$_6$H$_4$N)$_{14}$Ta$_6$O] (11)

Compound **3** (100 mg, 0.0388 mmol, 1.00 equiv) was dissolved in 10 mL of hot toluene. A solution of decamethylcobaltocene (20 mg, 0.061 mmol, 1.5 equiv) in 3 mL of toluene was then added, resulting in a dark brown-green solution from which **11** began to precipitate upon cooling to ambient temperature. The reaction vessel was cooled at −30 °C overnight. The green supernatant was removed by filtration, and the amorphous product (93 mg, 0.032 mmol, 82%) was washed with toluene (4 × 10 mL) and then 10 mL of pentane. Prior to submission for elemental analysis, material was crystallized by diffusion of pentane vapor into a THF solution of **11**. ^{1}H NMR (500 MHz, THF-d_8): δ 7.97 (br, 12H, *o*-terminal *Ar*), 6.00 (br, 16H, *m*-bridging *Ar*), 5.56 (br, 12H, *m*-terminal *Ar*), 5.35 (s, 24H, bridging Ar*Me*), 3.54 (v br, *o*-bridging *Ar*), 2.42 (v br, *Cp**), 0.31 (s, 18 H, terminal Ar*Me*). Assignments were determined by COSY NMR and comparison with spectra of **10**. μ_{eff}) 1.786 μ_B (295

K). Anal. Calcd for $C_{118}H_{128}CoN_{14}OTa_6$: C, 48.82; H, 4.44; N, 6.75. Found: C, 49.02; H, 4.79; N, 6.81.

Reaction of 3 with Benzophenone

Compound **3** (100 mg, 0.0388 mmol, 1.00 equiv) was dissolved in 10 mL of benzene. Benzophenone (99.0 mg, 0.543 mmol, 14.0 equiv) was then added, and the reaction mixture was transferred to a Pyrex reaction vessel fitted with a vacuum stopcock and heated at 135 °C for 24 h. Upon cooling, the white precipitate that had formed was removed by filtration and the solvent was removed from the filtrate under vacuum, yielding a yellow oil. A crystalline solid (127 mg, 0.468 mmol, 86%) was obtained after dissolution in and subsequent removal of pentane. Analysis of this material by ^{1}H NMR showed only benzophenone *p*-tolylketimine; its NMR and EIMS data matched those in the literature.51

Reaction of 3 with Benzaldehyde

Compound **3** (10 mg, 0.0039 mmol, 1.0 equiv) was dissolved in 0.5 mL of C_6D_6, and 5.5 μL (0.054 mmol, 14 equiv) of benzaldehyde was added by microsyringe. The mixture was transferred to an NMR tube and flame sealed under reduced pressure. The solution became orange in color after about 5 min, and the ^{1}H NMR spectrum obtained after 24 h showed that nearly all of the aldehyde had been converted to benzaldehyde *p*-tolylimine. Heating the NMR tube at 75 °C for 2 h converted the last traces of aldehyde. Additionally, a fine white precipitate had formed at the bottom of the vessel. The reaction mixture was then filtered, and the solvent was removed under vacuum. ^{1}H NMR and EIMS data matched the literature values for benzaldehyde *p*-tolylimine.51

Reaction of 3 with Acetophenone

Compound **3** (10 mg, 0.0039 mmol, 1.0 equiv) was dissolved in 0.5 mL of C_6D_6, and 6.3 μL (0.054 mmol, 14 equiv) of acetophenone was added by microsyringe. The mixture was transferred to an NMR tube and flame sealed under reduced pressure. After 3 d at ambient temperature, only resonances corresponding to acetophenone *p*-tolylimine (75 ± 5% yield by ^{1}H NMR) and one other, unidentified species were visible in the ^{1}H NMR spectrum. A fine white precipitate had also formed at the bottom of the vessel. The reaction mixture was filtered, and the solvent was removed under vacuum. ^{1}H NMR and EIMS spectra of the major product matched those in the literature for acetophenone *p*-tolylimine.52

Supplemental Material

Refer to Web version on PubMed Central for supplementary material.

Acknowledgments

We are indebted to Dr. Fred Hollander and Dr. Allen Oliver at the UC Berkeley CHEXRAY X-ray crystallographic facility and Dr. Kathleen Durkin at the Molecular Graphics Facility (NSF Grant CHE-0233882) for crystallographic and computational consultation, respectively, as well as Dr. John Greaves at UC, Irvine, CA, for mass spectrometry data. We also thank Dr. Alexandr Shafir for providing a preliminary structure of **2** using Mo Kα radiation. This work was supported by NIH Grant GM-25459 to R.G.B. and DOE funding to J.A.

References

1. a) Wigley, DE. Progress in Inorganic Chemistry. Vol. 1994. Vol. 42. John Wiley & Sons Inc.; New York: p. 239-482.(b) Gade LH, Mountford P. Coord Chem Rev. 2001; 216:65–97.
2. Schrock RR, Hoveyda AH. Angew Chem, Int Ed. 2003; 42:4592–4633.
3. a) Glueck DS, Hollander FJ, Bergman RG. J Am Chem Soc. 1989; 111:2719–2721.(b) Glueck DS, Wu JX, Hollander FJ, Bergman RG. J Am Chem Soc. 1991; 113:2041–2054.(c) Mindiola DJ,

Hillhouse GL. J Am Chem Soc. 2001; 123:4623–4624. [PubMed: 11457258] (d) Takemoto S, Morita H, Kamikawa K, Matsuzaka H. Chem Commun. 2006:1328–1330.(e) Kogut E, Wiencko HL, Zhang LB, Cordeau DE, Warren TH. J Am Chem Soc. 2005; 127:11248–11249. [PubMed: 16089446] (f) Danopoulos AA, Wilkinson G, Sweet TKN, Hursthouse MB. J Chem Soc, Dalton Trans. 1996:3771–3778.(g) Dobbs DA, Bergman RG. J Am Chem Soc. 1993; 115:3836–3837.

4. (a) Li Z, Quan RW, Jacobsen EN. J Am Chem Soc. 1995; 117:5889–5890.(b) Groves JT, Takahashi T. J Am Chem Soc. 1983; 105:2073–2074.
5. (a) Walsh PJ, Baranger AM, Bergman RG. J Am Chem Soc. 1992; 114:1708–1719.(b) Haak E, Bytschkov I, Doye S. Angew Chem, Int Ed. 1999; 38:3389–3391.(c) Shi YH, Ciszewski JT, Odom AL. Organometallics. 2001; 20:3967–3969.(d) Tillack A, Castro IG, Hartung CG, Beller M. Angew Chem, Int Ed. 2002; 41:2541–2543.
6. (a) Johnson JS, Bergman RG. J Am Chem Soc. 2001; 123:2923–2924. [PubMed: 11456996] (b) Li YH, Shi YH, Odom AL. J Am Chem Soc. 2004; 126:1794–1803. [PubMed: 14871111] (c) Baranger AM, Walsh PJ, Bergman RG. J Am Chem Soc. 1993; 115:2753–2763.
7. Anderson LL, Arnold J, Bergman RG. Org Lett. 2004; 6:2519–2522. [PubMed: 15255680]
8. One example of a V(IV) system exists; see the following: Lorber C, Choukroun R, Vendier L. Organometallics. 2004; 23:1845–1850.
9. The preliminary structure was provided by Dr. Alexandr Shafir.
10. While only a central O^{2-} would result in a neutral complex, the charge resulting from the presence of N^{3-} could be balanced by an as-yet unobserved cation in the lattice.
11. (a) Pope MT, Mueller A. Angew Chem, Int Ed Engl. 1991; 30:34–48.(b) Gouzerh P, Proust A. Chem Rev. 1998; 98:77–111. [PubMed: 11851500]
12. (a) Strong JB, Yap GPA, Ostrander R, Liable-Sands LM, Rheingold AL, Thouvenot R, Gouzerh P, Maatta EA. J Am Chem Soc. 2000; 122:639–649.(b) Clegg W, Errington RJ, Fraser KA, Holmes SA, Schaefer A. J Chem Soc, Chem Commun. 1995:455–456.(c) Kang H, Zubieta J. J Chem Soc, Chem Commun. 1988:1192–1193.
13. (a) Kessler VG, Seisenbaeva GA. Inorg Chem Commun. 2000; 3:203–204.(b) Decker A, Fenske D, Maczek K. Angew Chem, Int Ed Engl. 1996; 35:2863–2866.
14. Krinsky JL, Anderson LL, Arnold J, Bergman RG. Angew Chem, Int Ed. 2007; 46:369–372.
15. Advanced Light Source beamline 11.3.1, Lawrence Berkeley National Laboratory, operated under DOE contract DE-AC03-76SF00098.
16. Pickhard F, Hartl H. Z Anorg Allg Chem. 1997; 623:1311–1316.
17. Atmospheric pressure chemical ionization mass spectrometry, THF matrix.
18. Extension of B3LYP by Xu and Goddard to include the Perdew-Wang 1991 gradient exchange correction.
19. Schreiner PR. Angew Chem, Int Ed. 2007; 46:4217–4219.
20. (a) Uhl W, Cuypers L, Kaim W, Schwederski B, Koch R. Angew Chem, Int Ed. 2003; 42:2422–2423.(b) Heise H, Kohler FH, Herker M, Hiller W. J Am Chem Soc. 2002; 124:10823–10832. [PubMed: 12207538] (c) Braga D, Eckert M, Fraccastoro M, Maini L, Grepioni F, Caneschi A, Sessoli R. New J Chem. 2002; 26:1280–1286.
21. Duncan AP, Bergman RG. Chem Rec. 2002; 2:431–445. [PubMed: 12469354]
22. Blake RE Jr, Antonelli DM, Henling LM, Schaefer WP, Hardcastle KI, Bercaw JE. Organometallics. 1998; 17:718–725.
23. Strong JB, Ostrander R, Rheingold AL, Maatta EA. J Am Chem Soc. 1994; 116:3601–3602.
24. Bonanno JB, Wolczanski PT, Lobkovsky EB. J Am Chem Soc. 1994; 116:11159–11160.
25. Neithamer DR, Lapointe RE, Wheeler RA, Richeson DS, Vanduyne GD, Wolczanski PT. J Am Chem Soc. 1989; 111:9056–9072.
26. (a) Thomas IM. Can J Chem. 1961; 39:1386–1389.(b) Bradley DC. Coord Chem Rev. 1967; 2:299–318.
27. (a) Lewis LN, Garbauskas MF. Inorg Chem. 1985; 24:363–366.(b) Boyle TJ, Gallegos JJ, Pedrotty DM, Mechenbier ER, Scott BL. J Coord Chem. 1999; 47:155–171.(c) Johansson A, Roman M, Seisenbaeva GA, Kloo L, Szabo Z, Kessler VG. J Chem Soc, Dalton Trans. 2000:387–394.

28. (a) Walsh PJ, Hollander FJ, Bergman RG. Organometallics. 1993; 12:3705–3723.(b) Royo P, Sanchez-Nieves J. J Organomet Chem. 2000; 597:61–68.(c) Hanna TE, Keresztes I, Lobkovsky E, Bernskoetter WH, Chirik PJ. Organometallics. 2004; 23:3448–3458.(d) Guiducci AE, Boyd CL, Mountford P. Organometallics. 2006; 25:1167–1187.
29. (a) Jolly M, Mitchell JP, Gibson VC. J Chem Soc, Dalton Trans. 1992:1331–1332.(b) Wang WD, Espenson JH. Inorg Chem. 2002; 41:1782–1787. [PubMed: 11925170] (c) Gibson VC, Graham AJ, Jolly M, Mitchell JP. Dalton Trans. 2003:4457–4465.
30. Holland PL, Andersen RA, Bergman RG. Organometallics. 1998; 17:433–437.
31. Herrmann WA, Weichselbaumer G, Paciello RA, Fischer RA, Herdtweck E, Okuda J, Marz DW. Organometallics. 1990; 9:489–496.
32. Burland MC, Pontz TW, Meyer TY. Organometallics. 2002; 21:1933–1941.
33. Alaimo PJ, Peters DW, Arnold J, Bergman RG. J Chem Ed. 2001; 78:64.
34. Herrmann WA, Floel M, Kulpe J, Felixberger JK, Herdtweck E. J Organomet Chem. 1988; 355:297–313.
35. Compound **2** (synchrotron): APEX2: Area-Detector Software Package, version 1.0.27. Bruker AXSMadison, WI1995–99SMART: Area-Detector Software Package, version 5.631. Bruker AXSMadison, WI1995–99
36. Compound **2** (synchrotron): SAINT: SAX Area-Detector Integration Program, version 7.06. Siemens Industrial Automation IncMadison, WI2005SAINT: SAX Area Detector Integration Program, version 7.07B. Siemens Industrial Automation IncMadison, WI2005
37. XPREP, version 6.12. Bruker AXS; Madison, WI: 2001. (part of the *SHELXTL Crystal Structure Determination Package*)
38. SADABS: Siemens Area Detector ABSorption Correction Program, version 2.10. Bruker AXS; Madison, WI: 2005.
39. Sheldrick, G. SHELXTL Crystal Structure Determination Package. Bruker AXS; Madison, WI: p. 1995-1999.
40. Farrugia LJ. J Appl Crystallogr. 1997; 30:565.
41. *POV-ray*, v.3.5.icl.win32, copyright 1996–2002.
42. Jaguar, version 6.5. Schrodinger, LLC; New York: 2005.
43. Maestro, version 7.5. Schrodinger, LLC; New York: 2005.
44. Xu X, Goddard WA III. Proc Natl Acd Sci USA. 2004; 101:2673–2677.
45. Becke AD. J Chem Phys. 1993; 98:5648–5652.
46. Miehlich B, Savin A, Stoll H, Preuss H. Chem Phys Lett. 1989; 157:200–206.
47. Perdew JP, Chevary JA, Vosko SH, Jackson KA, Pederson MR, Singh DJ, Fiolhais C. Phys ReV B. 1992; 46:6671–6687.
48. Stephens PJ, Devlin FJ, Chabalowski CF, Frisch MJ. J Phys Chem. 1994; 98:11623–11627.
49. Hay PJ, Wadt WR. J Chem Phys. 1985; 82:299–310.
50. (a) Ditchfield R, Hehre WJ, Pople JA. J Chem Phys. 1971; 54:724–728.(b) Hehre WJ, Ditchfield R, Pople JA. J Chem Phys. 1972; 56:2257–2261.(c) Hariharan PC, Pople JA. Theor Chim Acta. 1973; 28:213–222.(d) Francl MM, Pietro WJ, Hehre WJ, Binkley JS, Gordon MS, DeFrees DJ, Pople JA. J Chem Phys. 1982; 77:3654–3665.
51. Nongkunsarn P, Ramsden CA. Tetrahedron. 1997; 53:3805–3830.
52. Barluenga J, Fernandez MA, Aznar F, Valdes C. Chem–Eur J. 2004; 10:494–507. [PubMed: 14735518]

NIH-PA Author Manuscript
NIH-PA Author Manuscript

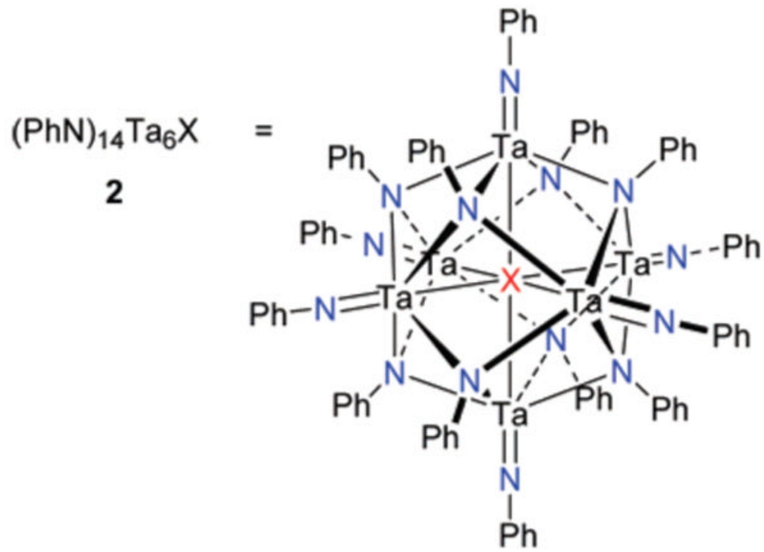

Figure 1.

Preliminary structure of octahedral hexatantalum cluster **2** (X = O or N). Other unidentified fragments are present in the unit cell.

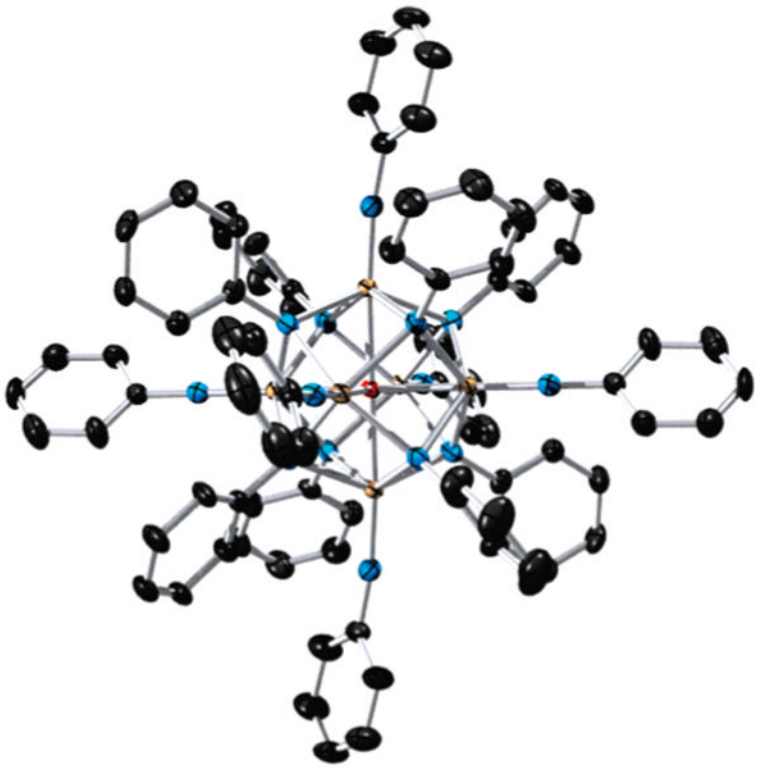

Figure 2.
ORTEP diagram of $(PhN)_{14}Ta_6O$ (**2**) at 50% probability. H atoms are omitted for clarity. Legend: C, black; N, blue; O, red; Ta, gold. Bond lengths (Å): Ta–O 2.2079(4), 2.2035(5), 2.2119(4); $Ta–N_{terminal}$ 1.790(3), 1.793(4), 1.791(4).

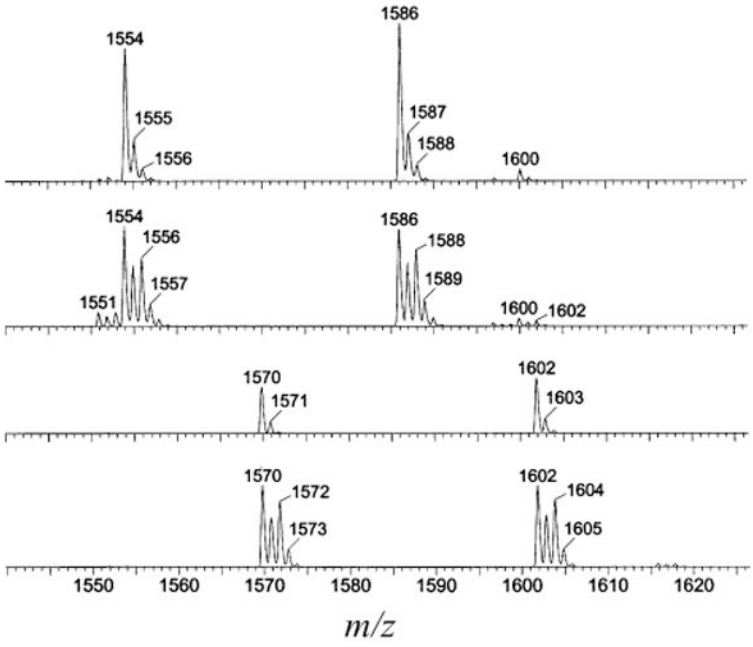

Figure 3.

Selected region of ESI mass spectra of **3**, **3**(^{17,18}O), **4**, and **4**(^{17,18}O) (top to bottom, respectively). Additional peak intensities are shown at $(m + 1)/z$ and $(m + 2)/z$ in spectra of isotopically labeled samples.

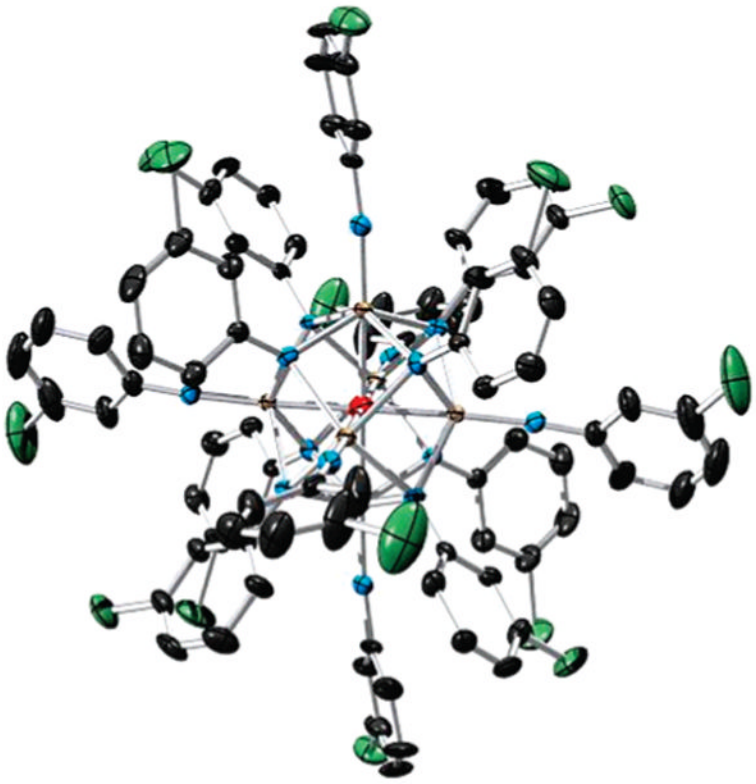

Figure 4.
ORTEP diagram of (*m*-$ClC_6H_4N)_{14}Ta_6O$ (**7**) at 50% probability. H atoms are omitted for clarity. Legend: C, black; Cl, green; N, blue; O, red; Ta, gold. Bond lengths (Å): Ta–O 2.1741(2), 2.1808(2), 2.1658(2); $Ta–N_{terminal}$ 1.811(4), 1.806(4), 1.811(4).

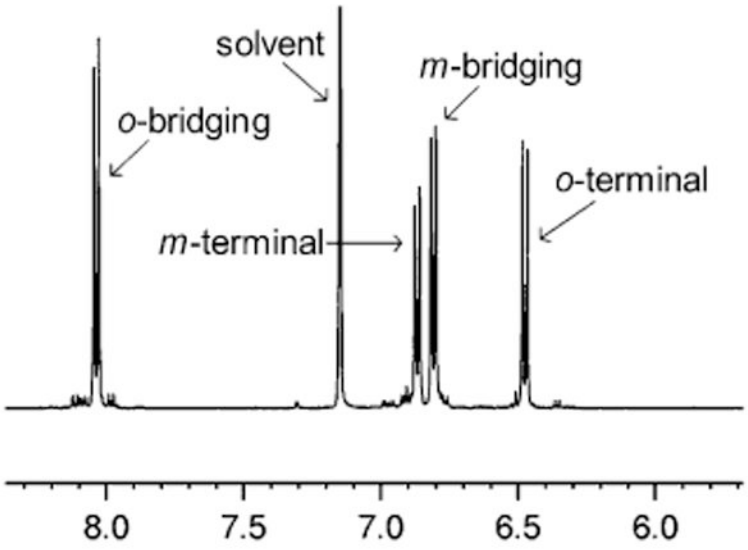

Figure 5.
^{1}H NMR spectrum of **3** in C_6D_6, aryl region only. All bridging or terminal phenylimido groups are spectroscopically equivalent.

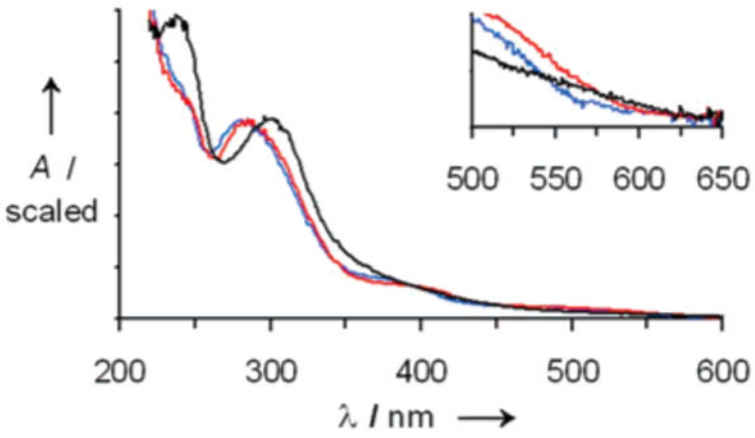

Figure 6.
UV–visible absorption spectra of **2**–**4** in THF. Legend: **2**, blue; **3**, red; **4**, black. Insert: visible-wavelength absorption onsets.

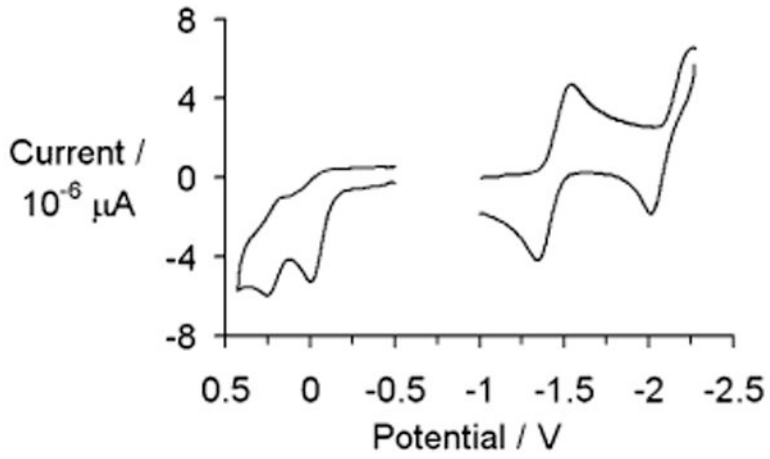

Figure 7.

Cyclic voltammogram of **3** in THF with 0.1 M $[Bu_4N][PF_6]$, with scan rate = 50 mV/s. Reductions: −1.44, −2.14 V. Oxidations: 0.01, 0.27 V (relative to Fc/Fc^+ couple).

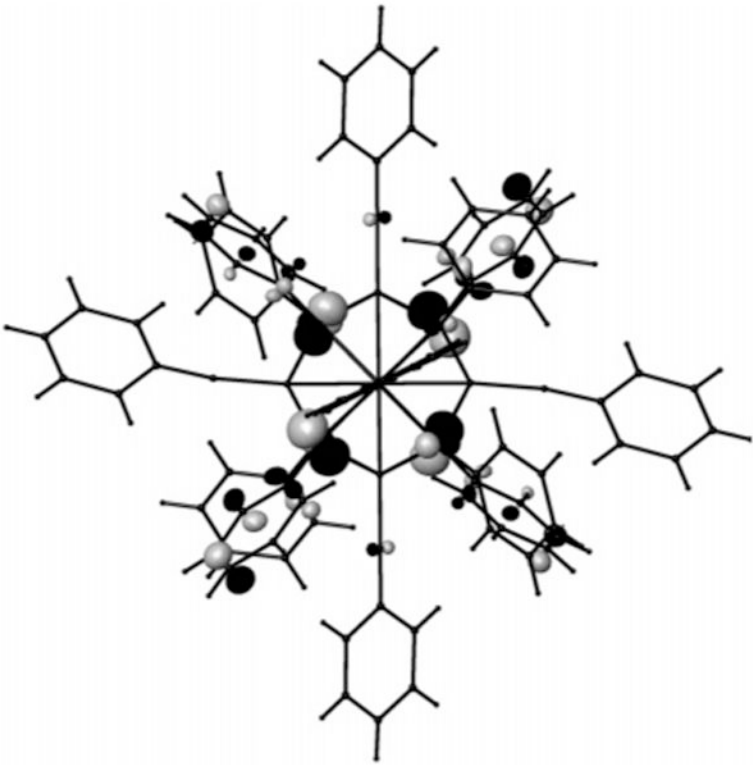

Figure 8.
Orbital diagram of the HOMO of **2**, calculated at the X3LYP/LACVP* level of theory using crystallographically determined coordinates.

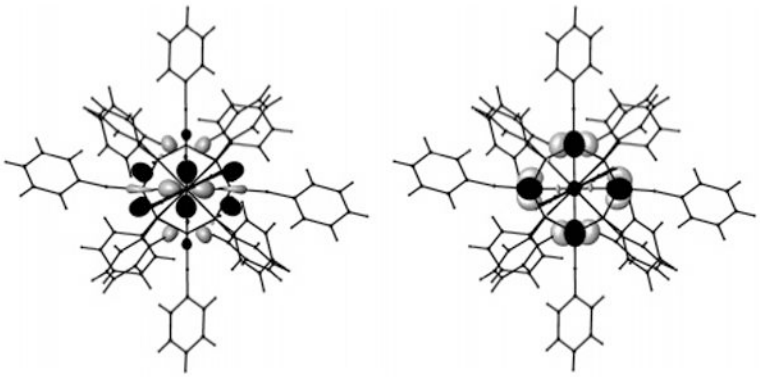

Figure 9.
Orbital diagrams of the LUMO (left) and LUMO+1 (right) of **2**, calculated at the X3LYP/LACVP* level of theory using crystallographically determined coordinates. The long axis of the cluster core is normal to the plane of the page.

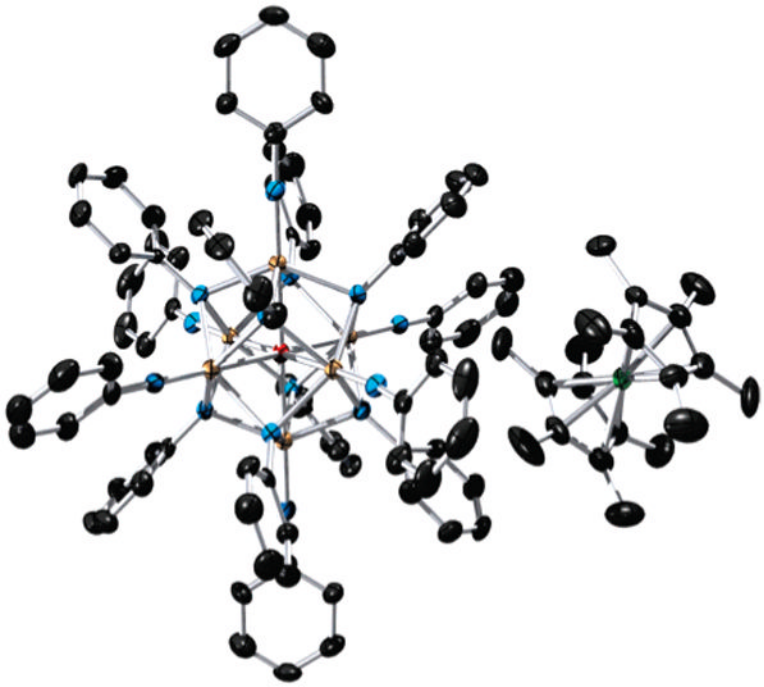

Figure 10.

ORTEP diagram of $[(PhN)_{14}Ta_6O][Cp^*_2Co]$ (**10**) at 50% probability. H atoms are omitted for clarity. Legend: C, black; Co, green; N, blue; O, red; Ta, gold. Bond lengths (Å): Ta–O 2.2018(4), 2.2099(4), 2.2120(4); $Ta–N_{terminal}$ 1.785(6), 1.788(6), 1.803(6); $Co–C_{ring}$ 2.041(9), 2.043(9), 2.043(9), 2.054(9), 2.054(8).

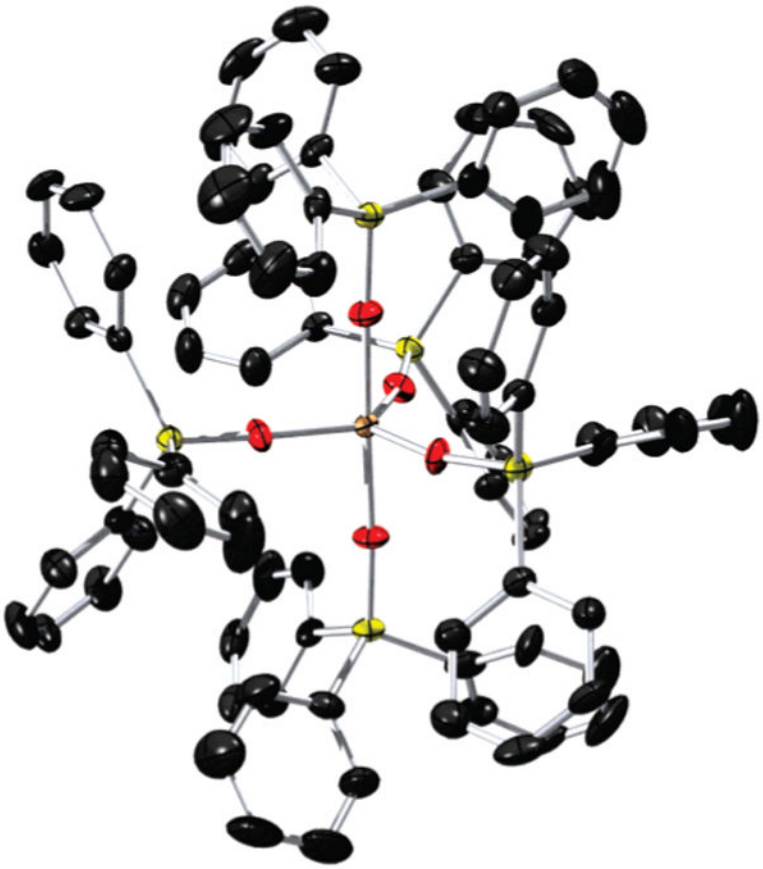

Figure 11.

ORTEP diagrams showing two views of $Ta(OSiPh_3)_5$ (**12**) at 50% probability. H atoms are omitted for clarity. Legend: C, black; O, red; Si, yellow; Ta, gold. Selected bond lengths (Å) and angles (deg): Ta1–O1, 1.949(6); Ta1–O2, 1.914(7); Ta1–O3, 1.886(5); Ta1–O4, 1.884(5); Ta1–O5, 1.889(5); O1–Ta1-O2, 178.1(4); O3–Ta1-O4, 118.2(3); O4–Ta1-O5, 119.1(2); O3–Ta1-O5, 122.7(2).

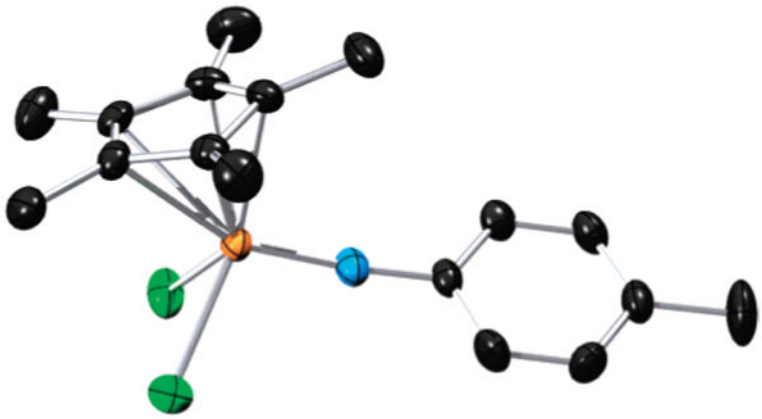

Figure 12.

ORTEP diagram of $Cp^*Cl_2Re{=}N\text{-}p\text{-}C_6H_4Me$ (**13**) at 50% probability. H atoms are omitted for clarity. Legend: C, black; Cl, green; N, blue; Re, orange. Selected bond lengths (Å) and angles (deg): Re1–N1, 1.726(4); Re1–Cl1, 2.3783(13); Re1–Cl2, 2.3845(13); Re1–C1, 2.217(5); Re1–C2, 2.178(5); Re1–C3, 2.224(5); Re1–C4, 2.415(5); Re1–C5, 2.405(4), N1–C11, 1.387(6); Re1–N1-C11, 171.5(3).

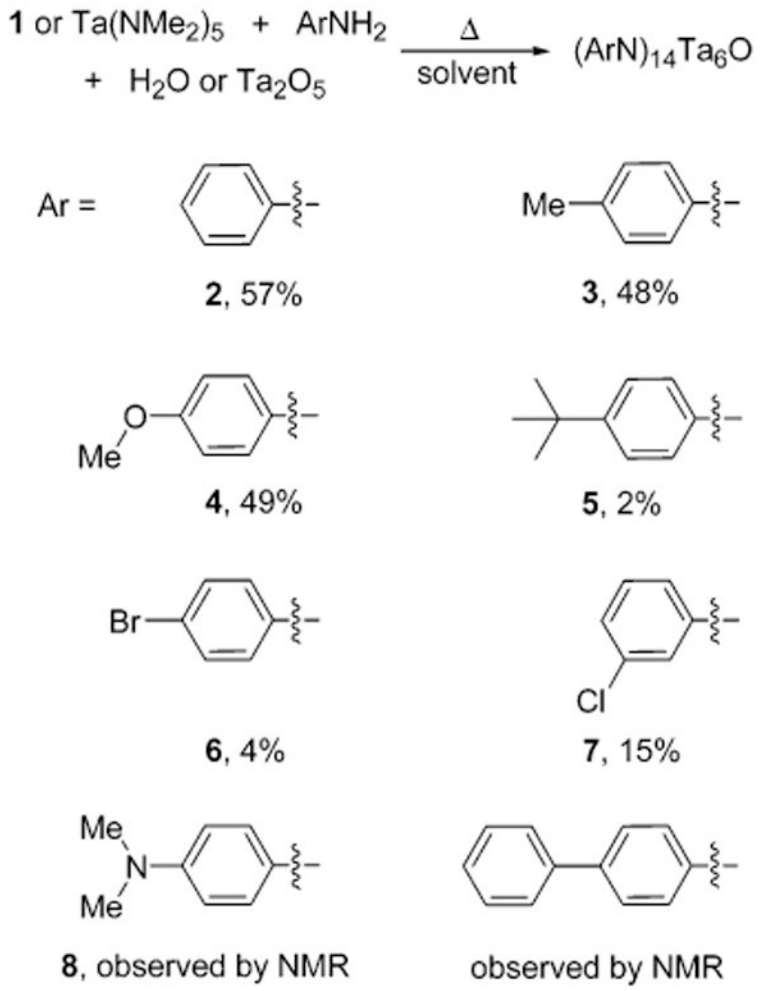

Scheme 1.

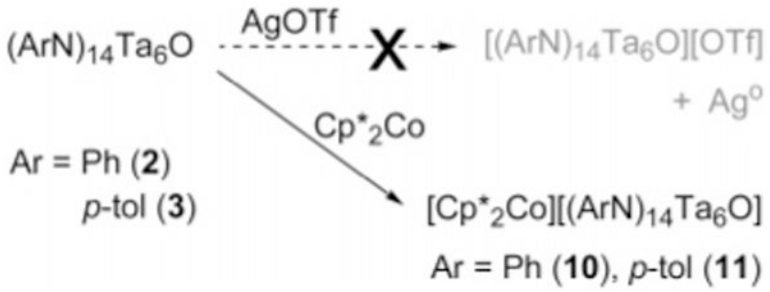

Scheme 2.

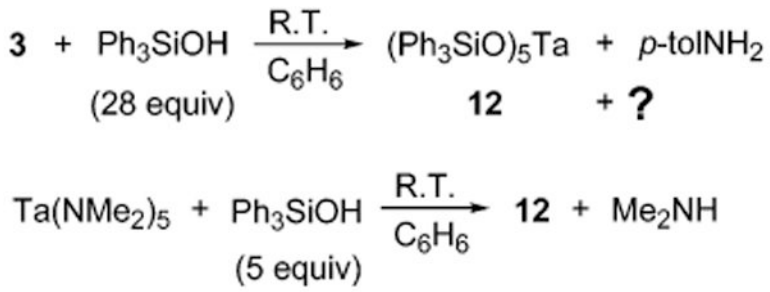

Scheme 3.

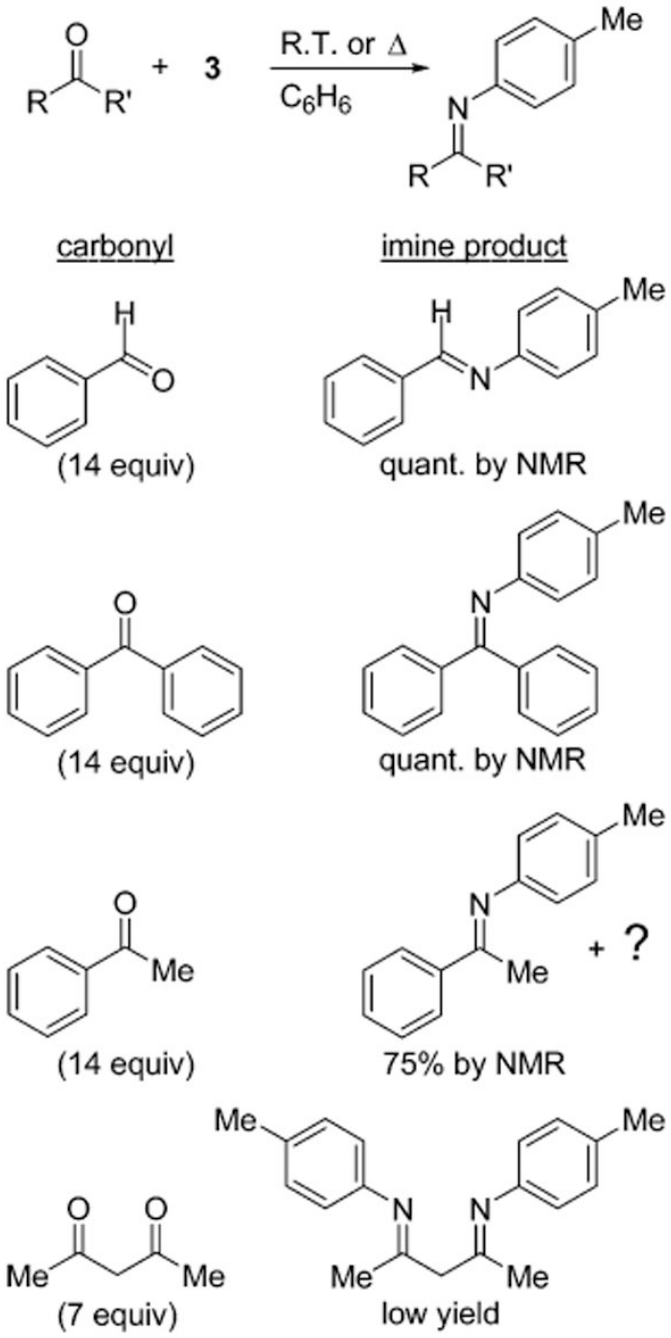

Scheme 4.

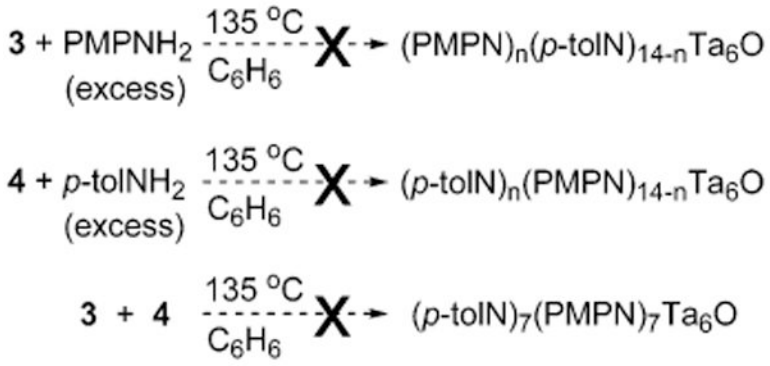

Scheme 5.

Table 1

Screen of Possible Trace Oxygen Sources, Added in Substoichiometric Quantities

entry	Ta source	additive[a]	solvent	yield of 2 (%)[b]
1	**1**		C_6H_6	trace
2	**1**	O_2	C_6H_6	0
3	**1**	O_2[c]	C_6H_6	0
4	**1**[d]		C_6H_6	5
5	**1**[d]	H_2O/O_2	C_6H_6	5
6	**1**	H_2O	C_6H_6	20
7	**1**	H_2O[c]	C_6H_6	0
8	**1**	$\mathbf{H_2}O$	$\mathbf{C_6}H_6$/hexane	57
9	**1**	Ta_2O_5	C_6H_6	36

[a] 0.2 equiv except Ta_2O_5.

[b] 0.2 mmol of **1**, 5 equiv of aniline, 5 mL of solvent, 135 °C, 48 h, N_2 atmosphere.

[c] Added after heating.

[d] Partially oxidized.

Table 2

MO Energies (eV) for X3LYP/LACVP*-Optimized **2**–**4** and **9**

orbital	9	2	3	4
HOMO	−7.06	−5.46	−5.18	−4.81
LUMO	−3.88	−2.51	−2.29	−2.11
HOMO–LUMO gap	3.18	2.95	2.89	2.70

Table 3

Crystallographic Data for Compounds **2** (Synchrotron), **2** (Mo Kα), **7**, and **10**

param	2 (synchro)	2 (Mo Kα)	7	10
space group	$P\bar{1}$	$P\bar{1}$	$P\bar{1}$	$C2/c$
a, Å	*14.137(3)*	*13.6126(17)*	*13.148(1)*	*24.989(2)*
b, Å	*14.262(2)*	*13.8895(17)*	*13.796(1)*	*15.2762(14)*
c, Å	14.343(3)	14.0722(17)	16.005(1)	29.288(3)
α, deg	76.192(4)	89.991(2)	108.687(1)	90
β, deg	72.097(4)	76.981(2)	96.277(1)	99.8360(10)
γ, deg	60.491(4)	61.835(2)	94.847(1)	90
V, Å^3	*2381.5(9)*	*2267.8(5)*	*2711.5(3)*	*11016.0(18)*
Z	1	1	1	4
ρ_{calcd}, g cm^{-3}	1.875	1.952	1.936	1.806
μ(Mo Kα), mm^{-1}	8.59[a]	7.27	6.43	6.14
F_{000}	1286	1278	1510	5820
cryst size, mm	*0.05* × *0.05* × *0.04*	*0.23* × *0.16* × *0.05*	*0.22* × *0.14* × *0.06*	*0.20* × *0.17* × *0.08*
T, K	193(2)	155(2)	168(2)	136(2)
θ range, deg	1.80–33.67	1.50–26.43	1.36–26.39	3.32–24.72
no. rflcns measd	32 552	14 361	15 509	27 405
no. indep rflcns	13 506	8933	10 598	9309
R_{int}	0.0600	0.0350	0.0196	0.0459
no. restraints, params	0, 583	0, 565	0, 617	0, 615
R_1, wR_2[b] (all)	0.0520, 0.1384	0.0726, 0.1069	0.0422, 0.0741	0.0673, 0.0939
R_1, wR_2 (obsd[c])	0.0501, 0.1359	0.0438, 0.0991	0.0303, 0.0713	0.0389, 0.0848
GOF[d] on F^2	1.026	1.035	0.997	1.049
largest diff peak, hole, e Å^{-3}	2.820, –2.150	3.041, –1.479	1.309, –1.065	1.809, –1.202

[a] λ = 0.774 90 Å (synchrotron radiation).

[b] $R1 = \Sigma||F_o| - |F_c||/\Sigma|F_o|$; $wR2 = [\Sigma w(F_o^2 - F_c^2)^2/\Sigma w(F_o^2)^2]^{1/2}$, $w = 1/[\sigma^2 F_o^2 + (ap)^2 + bp]$, $p = [F_o^2 + 2F_c^2]/3$.

[c] $I > 2\sigma(I)$.

[d] $GOF = [w(F_o^2 - F_c^2)^2/(n - p)]^{1/2}$.

Table 4

Crystallographic Data for Compounds **12** and **13**

param	12	13
space group	*Cc*	$P2_1/n$
a, Å	*22.873(3)*	*8.4832(15)*
b, Å	*13.937(2)*	*17.131(3)*
c, Å	26.999(4)	13.904(2)
α, deg	90	90
β, deg	107.564(3)	102.723(2)
γ, deg	90	90
V, Å^3	*8206(2)*	*1971.0(5)*
Z	4	4
ρ_{calcd}, g cm^{-3}	1.324	1.784
μ(Mo Kα), mm^{-1}	1.47	6.44
F_{000}	3360	1024
cryst size, mm	*0.22 × 0.19 × 0.16*	*0.12 × 0.08 × 0.05*
T, K	165(2)	157(2)
θ range, deg	1.58–26.38	3.37–24.71
no. rflcns measd	23 045	8687
no. indep rflcns	11 758	3334
R_{int}	0.0651	0.0257
no. restraints, params	2, 965	0, 223
R_1, wR_2[a] (all)	0.0616, 0.0998	0.0403, 0.0575
R_1, wR_2 (obsd[b])	0.0461, 0.0941	0.0256, 0.0544
GOF[c] on F^2	0.912	1.114
largest diff peak, hole, e Å^{-3}	1.660, −0.743	1.778, −0.981

[a] $R1 = \Sigma||F_O| - |F_C||/\Sigma|F_O|$; $wR2 = [\Sigma w(F_O^2 - F_C^2)^2/\Sigma w(F_O^2)^2]^{1/2}$, $w = 1/[\sigma^2 F_O^2 + (ap)^2 + bp]$, $p = [F_O^2 + 2F_C^2]/3$.

[b] $I > 2\sigma(I)$.

[c] $GOF = [w(F_O^2 - F_C^2)^2/(n-p)]^{1/2}$.